Devonian geodynamic evolution of the Variscan Belt, insights from the French Massif Central and Massif Armoricain

Michel Faure, Eugène Be Mezeme, Alain Cocherie, Philippe Rossi, Alexandre Chemenda, David Boutelier

Devonian geodynamic evolution of the Variscan Belt, insights from the French Massif Central and Massif Armoricain

Michel Faure

Institut des Sciences de la Terre d'Orléans, Université d'Orléans,
Orleans, France

Eugène Bé Mézème

Institut des Sciences de la Terre d'Orléans, Université d'Orléans,
Orleans, France

BRGM,
Orleans, France

Alain Cocherie and Philippe Rossi

BRGM,
Orleans, France

Alexandre Chemenda

Géosciences Azur, UMR CNRS 6526, Université de Nice-Sophia Antipolis,
Valbonne, France

David Boutelier

Géosciences Azur, UMR CNRS 6526, Université de Nice-Sophia Antipolis,
Valbonne, France

Abstract

[1] The Paleozoic French Variscan Belt in Massif Central and Massif Armoricain is a collision belt that provides a good example of a suture zone where ophiolites are rare, and the frontal (i.e., the magmatic arc) part of the upper plate is not present. In the lower plate (or Gondwana), the continental rocks are subdivided into an Upper Gneiss Unit (UGU) and a Lower Gneiss Unit (LGU). The UGU experienced a high-pressure (and likely ultra-high-pressure) metamorphism followed by crustal melting during their exhumation. New chemical U-Th-Pb monazite ages and ion-probe U-Pb zircon ages on migmatites allow us to constrain the P-T-t paths followed by the UGU and LGU. By comparison with thermomechanical experiments, a possible geodynamic evolution scenario can be proposed for the Variscan convergence. The high-compression regime of continental subduction developed during the initial subduction of the northern margin of Gondwana under Armorica in Silurian times. This induced the formation of a new subduction zone in the back-arc basin, which is the youngest,

hottest, and thus mechanically the weakest part of the overriding plate. As a result, the arc-back-arc basin domain has been almost totally subducted below Armorica. Only a limited part of the back-arc basin rocks remains exposed in the Devonian St-Georges-sur-Loire Unit. Subsequently, the continental subduction of Gondwana resumed with a steeper dip associated with low-compression regime that in turn allowed the high-pressure rocks to be exhumed and partly melted in Late Devonian times. Such a scheme depicts quite well the complexity of the Variscan Belt.

Keywords: continental subduction, exhumation of HP rocks, U-Th-Pb geochronology, magmatic arc subduction, crustal melting, French Variscan Belt.

1. Introduction

[2] It is now widely accepted that in collision belts, continental crust of the underlying plate usually experienced deep-seated subduction. The occurrence of ultra-high-pressure (UHP) minerals such as coesite or diamond, included in garnets, attests for the burial of supracrustal sedimentary and magmatic rocks at depth larger than hundred of kilometers [e.g., Carswel and Zhang, 1999; Chopin, 2003; Liu et al., 2004, and references therein]. Since these rocks presently crop out in the core of orogens, the question of the mechanisms responsible for their exhumation represents a crucial point to solve for improving our understanding of orogenic processes. Furthermore, in collision orogens, crustal melting is also commonly developed. Erosion, horizontal contraction, tectonic denudation by low-angle normal faulting, or vertical extrusion are some of the most popular mechanisms frequently invoked to account for the unroofing of deep seated metamorphic rocks during or after orogeny [e.g., Wernicke and Burchfiel, 1982; Dewey, 1988; Lister and Davis, 1989; Malavieille, 1993; Chemenda et al., 1995].

[3] Analogue mechanical modeling has shown that, coeval with continental subduction, the buoyancy-driven rise of a coherent crustal wedge may be an efficient process [e.g., Chemenda et al., 1995, 1996, 1997]. Another important insight derived from thermomechanical modeling is that, depending on the boundary conditions, the upper plate can also experience severe deformations. In particular, it has been shown that a magmatic arc installed upon the overriding lithosphere and separated from the main part of the upper plate by a back-arc basin, can be partly or totally subducted during collision [Boutelier et al., 2003]. These results have been successfully applied to natural cases, such as Oman, Himalayas, Urals or Taiwan [Chemenda et al., 1995, 1997, 2001; Boutelier et al., 2003].

[4] In this paper, we present new geochronological data obtained from the Western part of the Variscan French Massif Central related to crustal melting during the exhumation of high-pressure units and we explore the possibilities suggested by analogue thermomechanical modeling to explain the exhumation of the deeply buried continental crust involved in the Paleozoic French Variscan Belt. We argue that the southern margin of the upper plate (called Armorica) consisted of a magmatic arc and back-arc system that have been almost totally subducted during continental collision with the lower plate (or northern Gondwana). Arc subduction is responsible for the switch from high- to low-compression mode that allows crustal melting during the exhumation of HP rocks.

2. Geological Outline of the French Variscan Belt

[5] The Variscan Belt that forms the basement of Medio-Europa experienced a long-standing evolution from Cambrian-Ordovician rifting to Carboniferous final amalgamation and orogenic collapse [e.g., Matte, 1986, 2001; Faure et al., 2005, and references therein]. In France, the Variscan Belt is well exposed in the Massif Central and Massif Armoricain (Figure 1). There, two contrasted paleogeographic and tectonic domains are recognized. The Nort-sur-Erdre Fault (Figures 1 and 2) corresponds to the suture zone between the Armorican Domain and the North Gondwana Margin Domain, to the North and South, respectively. In this section, the main features of each domain are presented, and then details on the suture zone are provided.

2.1. Armorican Domain

[6] The area occupied by Central and Northern Brittany belongs to the Armorica microcontinent [Matte, 2001]. It consists of Neoproterozoic rocks metamorphosed and deformed during the Neoproterozoic Cadomian orogeny, around 600−550 Ma, and unconformably covered by unmetamorphosed and weakly deformed Paleozoic sedimentary series. The main Variscan structure of Central Brittany consists of E–W trending upright folds associated to dextral wrenching of Middle to Late Carboniferous age. The North Armorican Shear Zone (NASZ), North Branch of the South Armorican Shear Zone (NBSASZ), and South Branch of the South Armorican Shear Zone (SBSASZ) are the main wrench faults that accommodate this dextral shearing (Figure 1). In the Armorican Domain, Carboniferous formations are restricted to E–W elongated basins, located along the NASZ. In spite of a severe Middle to Late Carboniferous wrench-related deformation, an Early Carboniferous unconformity attests for an earlier event recognized for a long time as the “Bretonian phase” [e.g., Cogné, 1974; Rolet, 1982; Le Gall et al., 1992].

[7] Between the NBSASZ and the Nort-sur-Erdre suture zone, the southern margin of Armorica is highly tectonized. There, the Paleozoic rocks are ductilely deformed by flat-lying shear zones and NW–SE trending mineral and stretching lineations associated with a top-to-the-NW ductile shearing. North to NW-vergent folds coeval with gently dipping axial planar slaty cleavage are also developed [Ledru et al., 1989; Cartier and Faure, 2004] (Figure 2a). Two tectonic units, namely the Lanvaux and St-Georges-sur-Loire Units, are recognized. To the North, the Lanvaux Unit consists of Neoproterozoic rocks overlain by Cambrian terrigenous series and intruded by Early Ordovician granitoids transformed into orthogneiss. The Lanvaux Unit is overthrust to the NW by a block-in-matrix series called the St-Georges-sur-Loire Unit made of Silurian chert, Cambrian rhyolite, Devonian limestone, pillow basalt, gabbro, andesite, trachyte and sandstone. These various rock types are meter to kilometer-sized blocks enclosed into a turbiditic matrix composed of coarse-grained sandstone, siltstone, black mudstone, sandstone-mudstone alternations and pebbly mudstone [Lardeux and Cavet, 1994; Cartier, 2002; Cartier and Faure, 2004]. Geochemical studies of whole rock and minerals from gabbro, diabase, and basalt olistoliths, show the coexistence of tholeiitic basalts (E-MORB) and island arc-tholeiites, which are in agreement with an island arc setting [Cartier, 2002; Cartier and Faure, 2004, and references therein]. Furthermore, acidic lavas plot in the field of volcanic arc granite of Pearce et al. [1984].

[8] The age of the matrix is unsettled yet, however, Early Devonian blocks are the youngest rocks found in the sedimentary series, thus a Middle Devonian (Eifelian-Givetian) age has been proposed for the St-Georges-sur-Loire Unit [Cartier, 2002; Cartier and Faure, 2004].

Alike for the Lanvaux Unit, in the St-Georges-sur-Loire, the top-to-the-NW ductile shearing is coeval with a low-grade metamorphism conspicuously developed both in blocks and in matrix.

[9] Moreover, it is well acknowledged [e.g., Dubreuil, 1986; Cartier and Faure, 2004], that the faunal assemblages found in the Devonian limestone olistoliths enclosed in the St-Georges-sur-Loire Unit are quite different from those recovered in Central Brittany. This assessment led to the conclusion that these blocks derive from a presently disappeared domain located to the South of the St-Georges-sur-Loire Unit, which has been called "the Missing Domain" [Dubreuil, 1986; Cartier et al., 2001; Cartier and Faure, 2004]. A general geodynamic interpretation will be given at the end of this section.

2.2. North Gondwana Margin Domain

[10] The southern part of the Massif Armoricain and the entire Massif Central consist of metamorphic nappes stacked from North to South. In the Massif Central, five major units are recognized [e.g., Ledru et al., 1989; Faure et al., 2005]. Namely, from bottom to top, and South to North, they are (Figures 1 and 2b): (1) the Paleozoic Fold-and-Thrust Belt, (2) the Para-autochthonous Unit; (3) the Lower Gneiss Unit (LGU), (4) the Upper Gneiss Unit (UGU); and (5) the Thiviers-Payzac Unit.

[11] Owing to the diachronism in the timing of deformation, the first event experienced by the Fold-and-Thrust Belt and Para-autochthonous Unit occurred in Middle to Late Carboniferous times, from 340 Ma to 325 Ma [e.g., Matte, 1986; Faure et al., 2005]. Conversely, this event is not the first one recognized in the UGU and LGU. In the same way, the Thiviers-Payzac Unit that crops out in the S. part of the Limousin area (Figure 1) is involved only in the late stages of the orogenic evolution. Therefore, the Fold-and-Thrust Belt, Para-autochthonous and Thiviers-Payzac units will not be considered in the following. In Figures 1 and 2, the Para-autochthonous Unit and Lower Gneiss Unit are not distinguished, since the two units did not existed in Devonian.

[12] The UGU is characterized by paragneiss, orthogneiss and mafic rocks metamorphosed under high-pressure conditions. It is worth noting that the eclogite facies metamorphism affects both continental felsic and mafic rocks, but rocks derived from oceanic crust (i.e., ophiolites) are lacking in the UGU. Coesite bearing eclogites crop out in the Monts-du Lyonnais in Eastern Massif Central [Lardeaux et al., 2001]. It is likely that the whole UGU experienced such a UHP metamorphism coeval with continental subduction during the Variscan collision. Moreover, the UGU underwent a widespread crustal melting during its exhumation as presented in the next section.

[13] The LGU consists of Cambrian and Early Ordovician granitoids and grauwacke-pelite country rocks. Alike the UGU, the LGU underwent anatexis and synmetamorphic ductile deformation, called D1 event (see section 3). Up to now, this crustal melting was not dated. First chemical U-Th-Pb monazite dating of the Middle Devonian crustal melting is presented in section 4.

[14] The southern part of the Massif Armoricain, south of the Nort-sur-Erdre Fault is lithologically and structurally quite similar to the Massif Central (Figure 1). The lowermost unit that crops out in Vendée and around Nantes; that is, the Mauves Unit (Figure 3) is correlated with the LGU, since it is overlain by the UGU [Marchand, 1981; Ballèvre et al.,

1994; Faure et al., 2005]. It is overthrust by a stack of nappes that is presented below in section 2.3. The Thiviers-Payzac and Para-autochthonous Units crops out in Vendée (Figure 2a), but as for the Massif Central, the tectonic evolution of this unit during Carboniferous is beyond the scope of this paper.

2.3. Suture Zone

[15] The southern part of the Massif Armoricain, around Nantes, is the only place in France where the relationships between the Armorican Domain and the North Gondwana Margin Domain can be analyzed (Figure 3). According to our interpretation, the Nort-sur-Erdre fault is a plate boundary along which ophiolitic slices are preserved between Armorica and North Gondwana Margin. The area south of the Nort-sur-Erdre fault, sometimes called the Champtoceaux Complex, is recognized for a long time as a stack of nappes [e.g., Cogné, 1966]. Several tectonic units are distinguished, namely from North to South, or top to bottom: (1) the Mauges Nappe, (2) the Ophiolitic Nappe, (3) the UGU, and (4) the LGU (Figure 3).

[16] The Mauges Nappe consists of ductilely deformed Neoproterozoic rocks metamorphosed under greenschist facies conditions, and unconformably overlain by Cambrian to Ordovician undeformed terrigenous sedimentary rocks and acidic volcanics. This nappe overthrusts an Ophiolitic Nappe formed by metagabbro, amphibolite, serpentinized peridotite, micaschist and quartzite that probably represent recrystallized radiolarites. The magmatic and sedimentary rocks are called the Drain and the Havre Units, respectively [e.g., Marchand, 1981; Paquette, 1987; Ballèvre et al., 1994]. All these rocks are derived from an oceanic lithosphere. It is worth noting that both the Mauges Nappe and the Ophiolitic Nappe do not crop out in the Massif Central. The Ophiolitic Nappe is underlain by gneiss, micaschists and mafic rocks that experienced a HP metamorphism [Lasnier et al., 1973; Vidal et al., 1980; Ballèvre et al., 1994]. These metamorphic rocks are lithologically, petrologically and structurally quite similar to those of the UGU observed in the Massif Central. Alike in the Massif Central, migmatites developed at the expense of orthogneiss form the upper part of the UGU and enclose mafic blocks interpreted as unmelted parts of the protolith (Figure 4a). The available geochronological data will be presented in section 3.

[17] As in many orogens, the suture zone has been reworked as a wrench fault. The Nort-sur-Erdre suture moved as a left-lateral strike-slip fault along which the Late Tournaisian-Visean Ancenis basin opened as a pull-apart [e.g., Diot, 1980; Pelhate, 1994; Cartier and Faure, 2004]. This intramontane basin develops within the Mauges Nappe after its stacking upon the ophiolitic nappe.

[18] This brief outline shows that the present contact between Armorica and Gondwana Domains does not correspond to the primary tectonic arrangement. On the basis of lithological and structural studies, the geodynamic setting of the southern margin of Armorica can be interpreted in terms of an active plate margin [Cartier et al., 2001; Cartier and Faure, 2004]. As stated above, the Devonian limestones and the calc-alkaline magmatic rocks that crop out in the St-Georges-sur-Loire Unit are exotic blocks that cannot be supplied by a northern (i.e., Armorica) source, since there, the Devonian rocks present quite different facies. Conversely, a southern source, i.e., the “Missing Domain”, is more likely. Therefore, since arc-derived olistoliths are conspicuous, the block-in-matrix series of the St-Georges-sur-Loire Unit is interpreted as deposited in a back-arc basin (called the Layon Rift) located between Armorica, to the North, and a magmatic arc, to the South (called the Ligerian Arc) that was the source area of the exotic blocks.

3. Structural and Geochronological Constraints

[19] Several structural, metamorphic and magmatic events are distinguished in the French Variscan Belt (for a comprehensive review, see Faure et al. [2005]). In this section, emphasis is placed on the pre-Carboniferous D0 and D1 events.

3.1. Early Event (D0)

[20] The ductile deformation coeval with the high-pressure metamorphism is referred here to as the D0 event [Faure et al., 2005]. The eclogites and orthogneiss observed in the UGU are foliated and lineated, but detail structural studies are rare [e.g., Godard and van Roermund, 1995] and never related to the geographic coordinates. Thus, the regional geometric pattern of the planar and linear structures, and their kinematics developed during the D0 event are not documented yet.

[21] A Late Silurian age of the HP metamorphism is determined in several places, both in the Massif Central and Massif Armorican by U-Pb method on zircon (Figure 1 and Table 1) [Vidal et al., 1980; Pin and Lancelot, 1982; Peucat et al., 1982; Ducrot et al., 1983; Pin and Peucat, 1986; Paquette et al., 1985, 1995]. As a whole, the radiometric ages range between 435 Ma and 408 Ma. More recently, the eclogites from the Champtoceaux Complex yielded Sm-Nd and U-Pb ages of 362 ± 25 Ma and 356 ± 8 Ma, respectively [Bosse et al., 2000]. On the basis of these radiometric dates, considered as the age of the HP metamorphism, a similar but younger evolution is proposed (M. Ballèvre, personal communication, 2006). The Late Devonian−Early Carboniferous period would be the time of nappe stacking and exhumation of the metamorphic rocks, then the Middle to Late Carboniferous, shallow water deposits unconformably cover the exhumed rocks.

[22] The geological significance of the young ages in the HP rocks has already been discussed [Faure et al., 1997, 2005; Cartier and Faure, 2004]. This 360 Ma age can alternatively be interpreted as that of a younger recrystallization since most of the eclogites are commonly retrogressed as amphibolites [Faure et al., 2005]. Furthermore, these eclogites crop out as pods within migmatite, which is dated at 387 ± 6 Ma by the chemical U-Th-Pb method on monazite [Cocherie et al., 2005] (Figure 3). Thus the 360 Ma age is not in agreement with all other dates of the HP event, but the significance of this discrepancy is not clearly understood yet.

3.2. Main Event (D1)

[23] The D0 event is not the main one responsible for the nappe structure of the study area. The first structural event well recognized in the UGU and LGU, D1 event, is represented by a widespread flat-lying foliation and a conspicuous NE–SW (N50°E to N70°E) trending mineral and stretching lineation (Figure 1). Top-to-the-SW ductile shearing, indicated by sigmoidal biotite, quartz pressure shadows or sigma-type porphyroclast systems, is coeval with a MP/MT metamorphism characterized in gneiss by biotite-garnet-fibrolitic sillimanite assemblage [Floc'h, 1983; Roig and Faure, 2000]. This structural and metamorphic D1 event develops in ortho and paragneiss, but also in diatexites and metatexites formed at the expense of that gneiss, both in UGU and LGU.

[24] In the UGU, the protoliths of the migmatites are Al-rich rocks such as orthogneiss or metagreywacke. Conversely, the Fe-rich metabasites metamorphosed under eclogite facies

conditions during the D0 event were retrogressed as garnet amphibolites during the D1 event. The retrogression is a dynamic process responsible for the development of planar and linear preferred mineral orientation. $^{40}Ar/^{39}Ar$ ages of biotite and amphibole are available from amphibolite of the UGU [Costa and Maluski, 1988; Boutin and Montigny, 1993] (Table 1). The 390−380 Ma dates are considered as the timing of the retrogression of eclogites. The age of the anatexis of the UGU is presently settled in several areas of the Massif Central and Massif Armoricain (Table 1). U-Pb, Rb-Sr and U-Th-Pb methods show convergent Early to Middle Devonian ages around 387−382 Ma [Lafon, 1986; Duthou et al., 1994; Cocherie et al., 2005]. In the LGU, the age of the crustal melting was not determined yet. In section 4, chemical U-Th-Pb ages on monazite from migmatite are provided and used to discuss a geodynamic model.

[25] In the Ophiolite Nappe that crops out along the Nort-sur-Erdre Fault in the South part of the Massif Armoricain (Figures 2 and 3), foliated and lineated gabbro, amphibolite and micaschist exhibit a polyphase deformation. Gabbro mylonites of the Ophiolite Nappe present a NE–SW (N50°E) trending stretching lineation along which asymmetric sigma-type porphyroclast systems developed from pyroxene clasts indicate a top-to-the-SW shearing (Figure 4b). Owing to their geometry and kinematics, this deformation is related to the D1 event. Moreover, extensional shear bands that exhibit a NW–SE trending striation also deform the foliation. The kinematics associated with the shear bands indicates that the NW side moved downward [Lagarde, 1978] (also M. Faure, personal data, 1996, 1997). This top-to-the-NW ductile shearing accommodates the exhumation of the Ophiolitic Nappe and the UGU.

[26] As indicated by the radiometric ages (Table 1), the D0 and D1 tectono-metamorphic events are pre-Carboniferous in age. Moreover stratigraphic data comply with this statement. In the NE part of the Massif Central, or Morvan area (Figure 1), a Late Devonian series of unmetamorphosed limestone and sandstone crop out in close vicinity to gneiss, eclogites and migmatites of the UGU. Although the unconformity cannot be observed directly, the unconformable relationship between UGU and the Devonian sedimentary series appears likely (see discussion by Leloix et al. [1999] and Faure et al. [2005]). In Vendée area, the undeformed Villedé d'Ardin Middle Devonian (Givetian) limestone that crops out near the UGU HP rocks. This observation also supports a pre-Middle Devonian age of the D0 and D1 events.

[27] The Devonian events are followed by two tectonic and metamorphic events, called D2 and D3 that took place in Early and Middle Carboniferous, respectively. The D2 event, which is characterized by the development of a flat-lying foliation and a NW–SE trending stretching lineation, took place in Early Carboniferous. In the western part of the Massif Central, monzogranite plutons emplaced at the end of D2. The D3 event, of Middle Carboniferous age, is restricted to the southern part of the Massif Central. Since this paper deals with the pre-Carboniferous evolution of the French Variscan Belt, the younger events are not described here; for details, see Faure et al. [2005] and references therein.

4. New Chronological Constraints of the LGU in the French Massif Central

4.1. Results on Crustal Melting of LGU

[28] Two samples of migmatite derived from orthogneiss belonging to the LGU in the Limousin area have been dated (Table 1 and Figure 1). Sample Li 5 (N 45°13′65″; E

1°41′30″) is a migmatitic leucosome formed by partial melting of an augen orthogneiss from the central part of the Tulle antiform (Figures 2 and 4c). Sample Li 9 (N 45°30′37″; E 1°35′42″) is a metatectic orthogneiss taken from the southern limb of the Meuzac antiform (Figures 2 and 4d). The analyzed grains of monazite have been extracted from the quartz-feldspar rich leucosome layers in order to avoid the possibility of inherited grains. In thin section, both rocks are petrologically similar; owing to their chemical composition, the mineralogy is rather poor. A quartz-plagioclase-biotite assemblage formed during the crystallization of the melt surrounds relicts of K-feldspar augen derived from the orthogneissic protolith. Zircon, monazite, apatite, xenotime and oxides are the most common secondary phases. Monazite occurs as interstitial grain in the rock matrix between quartz and feldspar, along biotite grain boundaries or as inclusion in biotite (Figure 5). These textural relationships support the interpretation that monazite crystallized during crustal melting as the main mineral phases in the leucosomes. In the dated samples, Al-silicates are absent, but in the paragneiss and micaschist that form the orthogneiss host rock, oligoclase-biotite-garnet-sillimanite assemblage is commonly observed [Floc'h, 1983; Roig and Faure, 2000].

[29] The analyzed grains of monazite were extracted by crushing and sieving of ~400 g sample, followed by heavy liquids separation. Scan electron microscope (SEM) backscattered electron (BSE) images of the analyzed monazite grains from samples Li 5 and Li 9 are shown in Figures 6 and 7, respectively. Grains from sample Li 5 are more euhedral than those from sample Li 9. In both samples, grains are unaltered and present a patchy zoning related to relatively large variation in Th and U contents (Table 2 and auxiliary material). This kind of zoning is very common in monazite [e.g., Zhu and O'Nions, 1999; Cocherie et al., 2005; Santosh et al., 2006]. Conversely to zircon, typical concentric growth zoning is quite uncommon for monazite. The structure of the analyzed monazites is in agreement with their magmatic origin as indicated by the petrological observations.

[30] The uncertainty on a single age calculated from U, Th and Pb concentration is mainly a function of the amount of Pb, which in turn is depending of the amount of U + Th content. The simple counting statistic errors on each element can lead to underestimate the final uncertainty on a single U-Th-Pb age, particularly when U and Th contents are very high (see Cocherie and Legendre [2007] for details). To avoid it, we considered a minimum relative error of 2% for U and Th even for very high counting rates (see for instance sample Li 6). This minimum error takes into account other errors sources, such as standardization, matrix-effect correction and instrumental drift. Despite the application of this minimum error on Th content, monazite Li 6 shows very high Th contents (up to 19 wt%). Subsequently, high Pb content leads to relatively precise single age around ±30 Ma (2σ). On the contrary, low content of Th for samples Li 5 and Li 9 leads to higher uncertainties, around ±60 Ma and ±70 Ma respectively (annex). Therefore, despite the relatively wide range of individual age variation (Figures 6 and 7), all of them belong to the same age population within the uncertainty associated to the single ages.

[31] Analytical data are plotted in the U/Pb versus Th/Pb diagram [Cocherie and Albarède, 2001]. Detailed data are listed in the supplementary electronic material annex and a summary is given in Table 2 showing both the average and the range of variation for U, Th and Pb concentrations. The rather large U amounts associated to a significant Th/U variation in the monazites yields to a large spread of the data in the U/Pb versus Th/Pb diagram. It allows us to define a well-constrained regression line, as indicated by the error envelopes (Figures 8 and 9) . The regression lines are close to the theoretical isochron, indicating that the mean age can

confidently be calculated at the centroid of the population and that it is meaningful on a geochronological point of view. In other words, the theoretical Th-Pb and U-Pb ages, calculated at the intercepts of the regression line with the axis, are similar within the errors. Samples Li 5 and Li 9 yield ages of 378 ± 5 Ma and 374 ± 6 Ma, respectively that correspond to the time of crustal melting in the LGU.

4.2. Evidence for ~380 Ma Relictual Zircons in Granite

[32] The French Massif Central is intruded by several generations of granites. The oldest one corresponds to aluminous biotite ± cordierite monzogranite called "Guéret type" granites [e.g., Ledru et al., 1989; Faure, 1995; Faure et al., 2005]. Although sometimes magmatically foliated during their emplacement at the end of the D2 event [e.g., Roig et al., 1998], these plutons clearly postdate the D1 event described above in sections 2 and 3.

[33] The Guéret pluton itself is dated around 356−351 Ma both by Rb-Sr and U-Pb methods [Berthier et al., 1979; Cartannaz et al., 2006] (Table 1 and Figures 1 and 2). This radiometric age complies with stratigraphy since Early Carboniferous (Visean, ~340 Ma) limestone and terrigenous rocks unconformably overlie the Guéret massif. In the study area, the migmatitic series that form the core of the Tulle antiform is intruded by the Cornil pluton that belongs to the Early Carboniferous Guéret type pluton [Roig et al., 1998]. Monazite extracted from the Cornil pluton, (sample Li 6, N45°12′48″, E 1°41′28″) shows a high U content (Table 2) and an unusually high Th content (up to 19 wt%). As a result, each individual analysis yields a high Pb content (~2600 ppm) and a related low error on each individual ages. Moreover, the Th/U ratio does not change significantly. Then, the slope of the calculated regression line is associated to a quite large error. As a consequence, it is not surprising to observe that the regression line does not fit nicely with the theoretical isochron (Figure 10a). Nevertheless, since this population is quite homogeneous, a mean age can be calculated at the centroid of it, leading to an U-Th-Pb age of 359 ± 3 Ma (Figure 10a), which is in good agreement with ages of the Guéret-type granites.

[34] Eleven zircon grains from the same sample have been analyzed by IMS 1270 ion probe in CNRS CRPG laboratory in Nancy. Analyzed grains are generally elongated but they exhibit contrasting internal structure. The cathodoluminescence images of representative grains are shown on Figure 11. Zircon grains with large unaltered domains are rare. Some grains exhibit a core and rim structure, as grain 5 which yield $^{206}Pb^*/^{238}U$ ages at 443 ± 8 Ma and 336 ± 6 Ma respectively (all 2σ, Table 3). Grain 2 shows a magmatic growth zoning, but the two spot analyses yield 461 ± 8 Ma and 474 ± 8 Ma ages that do not correspond to the granite crystallization age inferred from other methods. These analyses probably do not suffer radiogenic Pb loss, but a large amount of common Pb was subtracted from the 2.1 analysis. Because of the scarcity of unaltered grains, five analyses were performed on grain 1 which is the clearest elongated one. It is part of a larger grain, probably broken during the separation process. No evidence of an inherited core can be shown in this well-crystallized grain. The analytic spots were placed sufficiently far from each other in order to avoid any analytical artifact. Nevertheless, only 3 analyses are similar within the analytical error (366 ± 10, 376 ± 8 Ma and 369 ± 12 Ma). Despite the quality of this grain, the two other spot analyses located toward the pyramid of the grain gave younger ages (351 ± 10 Ma and 330 ± 8 Ma). This age gap is interpreted here as the effect of radiogenic Pb loss. The well defined analyses of grain 3 are located right on the Concordia curve, indicating neither common Pb contribution nor radiogenic Pb loss, and thus an age at 382 ± 6 Ma can be calculated (Figure 10b and Table 3).

Grain 9 analysis yields to the same age at 380 ± 6 Ma after common Pb correction. Combining this group of 5 analyses, a mean $^{206}Pb^*/^{238}U$ age at 378 ± 7 Ma is calculated. Thus, in spite of a poor quality of the zircon population, in situ U-Pb study of the grains demonstrates that all of them are inherited, including a group of data giving ages ranging between 506 and 474 Ma, while a second group clusters around 378 Ma (Figure 10b). Lastly, the three analyses around 330 Ma are interpreted as the result of radiogenic Pb loss, they have no chronological significance.

[35] The available zircons did not experienced any significant recrystallization during the formation of the Cornil pluton which age is given by monazite dated at 359 ± 3 Ma. The ~380 Ma U-Pb age yielded by relict zircon grains is similar to the date derived from Li 5 migmatite sample that forms the Cornil pluton host rock. The Ordovician (480−470 Ma) age corresponds to that of the granite protolith, the melting of which produced the parent magma of the Cornil granite. Thus, zircon in the Cornil pluton attests for multiepisodic crustal melting of the Variscan continental crust.

5. Synthetic P-T-t Evolution of the UGU and LGU

[36] The above new chronological data combined with available chronological and thermo-barometric estimates both in the Massif Armoricain and Massif Central allows us to reconstruct the P-T-t paths for UGU and LGU (Figure 12).

[37] As stated in section 2, the prograde path of the UGU, is not documented. Maximum pressure condition measured in eclogitic rocks range from 20 to 28 kbar [e.g., Ballèvre et al., 1994; Godard, 2001; Lardeaux et al., 2001]. The retrogression of the UGU took place in nearly isothermal conditions. However, mafic, felsic and pelitic rocks experienced various retrogressive evolutions. During their ascent, the eclogites were retrometamorphosed to amphibolite, but only the pelitic rocks and felsic magmatic rocks underwent partial melting, owing to their Si-Al-rich composition. In the Limousin, P-T conditions of 7–8 kbar and 650°–750°C have been calculated for the oligoclase-biotite-garnet-sillimanite migmatite from the UGU [Floc'h, 1983; Roig and Faure, 2000]. The observation of relict kyanite surrounded by sillimanite suggests that these thermobarometric conditions are minimal values. Melting might have probably started under higher pressure in the stability field of kyanite. Several geochronological methods, namely whole rock Rb-Sr, TIMS on zircon single grains or chemical U-Th-Pb on monazite, provide similar ages around 387 ± 6 Ma–382 ± 5 Ma for the anatexis of the UGU (Table 1), whereas $^{40}Ar/^{39}Ar$ ages, about 389−381 Ma, of biotite and amphibole from retrogressed eclogites indicate an exhumation rate of about 2.5 km/Ma.

[38] The LGU paragneiss contains rare kyanite and plagioclase inclusions in garnet that indicate pressure conditions around 10–12 kbar, and the oligoclase-biotite-garnet-sillimanite assemblage in the gneiss matrix yield P-T conditions of 8–11 kb and 650 ± 50°C [Bellot, 2001]. However, alike for the UGU, these estimates probably do not reflect the maximum pressure conditions experienced by the LGU. Anatexis of the LGU took place around 378 ± 5 Ma to 375 ± 5 Ma (i.e., in Middle Devonian) during the retrogressive segment of the P-T path (Table 1). Therefore, petrological studies show that anatexis in both UGU and LGU developed under similar thermobarometric conditions at the kyanite-sillimanite transition, but crustal melting in the UGU might have started under higher-pressure conditions, earlier during its retrogression.

[39] In the present state of knowledge, the crustal melting of the UGU appears older of nearly 10 Ma than anatexis in the LGU. This time difference, close to the error bar (ca ± 5 Ma), can be only due to the limited amount of data, 4 and 3 from the LGU and UGU, respectively (Table 1). However, if the time difference is geologically significant, it suggests that crustal melting propagated through time from the UGU to the LGU, and subsequently from North to South, during the exhumation of the metamorphic units. Such a process would be in agreement with the tectonic scenario proposed in section 7.

6. Insights From Analogue Modeling

[40] As shown in the previous sections, the French Variscan Belt presents several noticeable features such as: (1) the stack of synmetamorphic nappes derived from the lower plate and displaced from NE to SW, and overthrusted by an Ophiolitic Nappe; (2) the widespread crustal melting developed in both UGU and LGU during their retrogression coevally with their exhumation; (3) the lack of a typical magmatic arc in the upper plate; and (4) the existence of the St-Georges-sur-Loire basin that contains sedimentary debris derived from a southern magmatic arc. Furthermore, monazite U-Th-Pb chemical ages bring chronological constraints on the crustal melting experienced by the LGU. All these points must be explained in any interpretative scenario. Moreover, in order to propose a reasonable geodynamic model it appears also necessary to take into account the physical aspects of lithosphere rheology. Experimental modeling can provide insights on the mechanical behavior and the coupling mode of the two converging plates.

[41] Analogue mechanical modeling of plate subduction [e.g., Chemenda et al., 1996] brought highly significant view on the exhumation of subducted continental crust. Thermomechanical modeling is a more realistic approach since temperature gradients and their influence on plate rheology are considered. Several models that took into account a complex overriding plate structure with a magmatic arc separated from the main part of the plate by a young back-arc basin and preceded by a fore-arc basin floored by oceanic crust have been already tested [Boutelier and Chemenda, 2003; Boutelier et al., 2003].

[42] In these experiments, the scenario of the arc-continent collision varies according to several parameters such as the total lithosphere thickness in the arc and back-arc spreading centre, arc strength and thermal gradients. For details on modeling setup, similarity criteria and chosen strength profiles, see Boutelier et al. [2003]. Models are characterized by an average arc thickness of ~26 km with a given rheology representative of an upper part of andesitic composition with terrigenous sediments and platform limestones. The lower part of the arc is assumed to be composed of granodioritic-dioritic plutons with high-strength rheology. The upper part of this lithological succession is in agreement with that recognized in the blocks enclosed in the St-Georges-sur-Loire Unit. The lithology of the lower crust is not unequivocally demonstrated since except gabbroic blocks, no plutonic element is identified in the St-Georges-sur-Loire Unit. Nevertheless, such a lithological composition for the magmatic arc remains a reasonable assumption.

[43] A possible scenario that satisfactorily accounts for the geological features of the Armorica-North Gondwana interactions is provided by “experiment 2” of Boutelier et al. [2003]. For relatively low thermal gradients and 25–30 km arc thickness, the coupling between crust and mantle is strong. The whole arc behaves as a single, relatively resistant, piece of lithosphere. The experiment (Figure 13) shows that during subduction of the continental margin, the overriding plate can fail in the arc area or near the back-arc basin-

spreading centre if the latter is the weakest part of the overriding plate. This scenario represents the case of a back-arc basin that was still opening just before the arrival of a continental margin in the subduction zone. In the case of Armorica, the age and geological history of the St-Georges-sur-Loire basin are not exactly known. As presented above, the Early Devonian limestone olistoliths show that the basin existed in Early to Middle Devonian. Evidence for an older age is not documented. In the model discussed in the following, a young back-arc basin is assumed since it is the only scenario allowing the total disappearance of the whole arc crust.

[44] In "experiment 2" (Figure 13), the subducting plate is composed of a normal, ~30 km, continental crust. The continental subduction causes an increase in the horizontal compression in the overriding plate. As a result, the upper plate fails in the back-arc basin. Then the subduction zone jumps to the failure location. Almost the total amount of plate convergence is accommodated in the new subduction zone, resulting in complete subduction of the arc plate, including the arc itself and a part of the back-arc lithosphere. Initial continental subduction first stops during this process and then restarts with a slower rate. The subducted arc plate plays a role of thermal shield protecting the subducted continental crust from the hot asthenosphere. This provides suitable conditions for the formation of UHP rocks. This process allows deeper subduction of the continental margin and relatively low temperatures are maintained in the subducted crust [Boutelier, 2004]. Then the UHP rocks are exhumed under buoyancy force when the continental crust reaches some critical depth and when interplate pressure is reduced [Boutelier, 2004]. At the end of the experiment, the whole arc-back arc segment of the upper plate is subducted into the asthenosphere. The final stage of the experiment presents similarities with the structure of the Massif Armoricain-Massif Central segment of the Variscan Belt (Figure 14). The UGU and LGU are derived from the subducted lower plate. The UGU experienced a high-pressure, or even an ultra-high-pressure metamorphism, and both the UGU and LGU experienced crustal melting during their exhumation. The Ophiolitic Nappe is a rather thin slice corresponding to the remnant of the oceanic domain located between Gondwana and Armorica. In the upper plate, the St-Georges-sur-Loire unit is the small preserved part of the back-arc basin that separated Armorica from the Ligerian magmatic arc. This last element has been entirely subducted below the Armorica plate.

7. A Possible Model for the Early Evolution of the French Variscan Belt

[45] In Late Ordovician−Early Silurian, ~450–430 Ma, the convergence between Armorica and North Gondwana margin led to the closure of the intervening Medio-European Ocean [e.g., Matte, 1986; Faure et al., 1997; Cartier and Faure, 2004]. As presented above, several lines of evidence support the existence of a complex architecture for the Armorica plate composed of the Ligerian magmatic arc separated from the main part of Armorica by the Layon Rift back-arc basin (Figure 15).

[46] In Middle to Late Silurian, ~430–410 Ma, the high-compression mode in the overriding plate, caused by the initiation of continental subduction, triggered failure of the Layon back-arc lithosphere since this is the place where the lithosphere is the thinner and the hotter. Since the back-arc basin is young, the back-arc spreading ridge area is mechanically the most likely place to initiate a new subduction zone.

[47] During Late Silurian-Early Devonian, ~410–390 Ma, the Layon Rift is closed, and only a very small part of this basin is presently preserved as the St-Georges-sur-Loire Unit. At the same time, the Ligerian Arc is subducted below Armorica. Indirect evidence for the existence of this magmatic arc is provided by olistoliths of calc-alkaline magmatic rocks and limestone that cannot be supplied by an Armorican source.

[48] Finally, in Late Devonian, ~390–370 Ma, when the arc plate is completely subducted, continuing convergence is accommodated by nappe stacking in two places. First, in the forearc domain, where the Ophiolitic Nappe overthrusts the UGU; and secondly, in the continental crust of Gondwana (i.e., S. Massif Armoricain and entire Massif Central) which is sliced into the UGU and LGU. Continental subduction results in scraping off and accretion of the upper layers of the continental crust at different depths. The thickness of the crust, remaining attached to the subducting lithospheric mantle, thus progressively reduces. This results in the increase in the slab pull which in turn, causes reduction of the interplate pressure and hence of the horizontal compression of the overriding plate. Whatever mechanism is responsible for the interplate pressure decrease, a switch from high- to low-compression regime must have happened, otherwise the exhumation of the UHP or HP/LT rocks would not have taken place.

[49] During the low-compression regime, the subducted crust fails at depth of several tens of kilometers where it is metamorphosed under UHP/LT conditions. The failure is followed by rapid rise of the deeply subducted crustal slices. The rising material experiences an isothermal decompression quickly followed by migmatization. The extrusion of the crustal wedge is accommodated by a top to the SW ductile shearing at its base and a top-to-the-NW ductile shearing on its top. As underlined in section 4, anatexis in the LGU might occur later (~10 Ma) than in the UGU. Such a time difference is in agreement with the southward propagation of crustal melting coeval with migration of deformation.

[50] This scenario accounts for the early evolution of the French Variscan belt. The younger Carboniferous events, such as pluton emplacement, strike-slip faulting or synmetamorphic shearing in the Para-autochthonous Unit are not discussed here. Seismic anisotropy and tomographic data obtained from the lithosphere mantle below the Massif Armoricain indicate the presence of a high-velocity mantle underlying the south part of Armorica [Granet et al., 2000]. Such a “cold and dense” body can be regarded as a remnant of the Ligerian Arc and the Layon Back-arc basin.

8. Conclusion

[51] The above reported new radiometric U-Th-Pb chemical dating of monazite from migmatites, combined with available thermobarometric estimates allow us to constrain the geodynamic evolution of the continental crust of the North Gondwana margin during the Variscan orogeny. The Middle Devonian crustal melting took place during the exhumation of a continental wedge subducted down to the eclogite facies conditions in Late Silurian-Early Devonian times. The Armorica upper plate consists of a rather thin and hot lithosphere with an arc-back-arc basin system. The comparison of the bulk architecture and kinematics of the suture zone between Armorica and Gondwana with thermomechanical models of continental subduction suggests that in the French Variscan Belt, the arc plate, including the arc itself and the back-arc lithosphere, has been subducted below Armorica. Presently, the St-Georges-sur-Loire Unit represents the highly tectonized and shortened remnant of the back-arc basin. The subduction of the magmatic arc is allowed by the low strength of the upper plate behind the

arc and the high-compression mode of continental subduction. Modeling experiments also suggest that buoyancy driven exhumation of the deeply subducted continental crust was allowed by the reduction of interplate pressure, i.e., owing to a switch from the high- to the low-compression mode of subduction regime.

[52] Subduction of a significant part of an overriding plate might be a quite widespread mechanism in many orogens. In the Variscan belt of Western Europe, the location of suture zones remains disputed [e.g., Paris and Robardet, 1990; McKerow et al., 2001; Robardet, 2003]. The disappearance by subduction of large parts of the upper plate edge, such as the magmatic arc, during continental convergence and collision may account for the complex geometry of plate boundaries and the difficulty to recognize the suture zones in orogenic belts.

Appendix A: Analytical Procedures

A1. EPMA Dating

[53] The electron probe microanalyzer (EPMA) is becoming increasingly popular for determining Th-U-Pb_{tot} ages on monazite because it provides a true in situ high spatial resolution method and because it is a nondestructive method. The studied monazite grains were extracted by crushing before being mounted in resin and polished, and then ready to be analyzed using a Cameca SX 50 electron microprobe (cooperated by BRGM and Orléans University, France). The analytical procedure for monazite was detailed in Cocherie et al. [1998, 2005]. The interference of YLγ on PbMα is subtracted offline by applying a coefficient of interference to the value of Y. The different interference corrections have been validated by dating several monazite samples using this method and using conventional isotopic methods [Cocherie et al., 1998]. An acceleration voltage of 20 kV was considered while a beam current of 100 nA is applied. According to this procedure, the calculated detection limits (2σ) is 150 ppm for Pb, U and for Th, whereupon an absolute error of 150 ppm is also taken. A systematic relative error of 2% is considered for Th (whose concentration is generally above 7500 ppm), and also for U concentrations above 7500 ppm in order to avoid an unrealistic low error for U-enriched grains [Cocherie and Legendre, 2007]. For monazite the standards were galena (PbS) for Pb, uraninite (UO_2) for U, thorite (ThO_2) for Th, end-member synthetic phosphates (XPO_4) for each rare earth element (REE) and Y, apatite for P and andradite for Si and Ca.

[54] If two or more homogeneous age domains are separated by a gap lower than the analytical error on each individual spot analysis age, these can be identified by suitable isochron diagrams [Suzuki and Adachi, 1991; Cocherie et al., 1998; Cocherie and Albarède, 2001]. A recent study shows how to provide precise ages of ±5 to 10 Ma (2σ) using the most suitable isochron diagram according to the geochemistry of the studied grains [Cocherie et al., 2005].

[55] With an obvious need for a program to simplify individual-age and isochron mean-age calculations, the EPMA dating, a Microsoft Excel add-in program for determining U-Th-$Pb_{tot.}$ ages from electron probe microanalyzer (EPMA) measurements has been created [Pommier et al., 2002]. All the parameters needed to calculate mean and intercept ages are computed, ready to be plotted, using the ISOPLOT program [Ludwig, 2000] in order to obtain statistics from suitable diagrams. Finally, EPMA dating produces (1) the U-Th-Pb age at the centroid of the best fit line, and (2) the Th-Pb age (intercept with Th/Pb axis) and the U-Pb age

(intercept with U/Pb axis) from the Th/Pb versus U/Pb diagram. All the calculations were done at 2σ levels. A special care was taken on the MSWD (Mean Squared Weighted Deviation) that must be below $1 + 2/(2/f)^{0.5}$ (f: degree of freedom = number of analyses - number of dated events) in order to validate age calculation [Wendt and Carl, 1991] for a single age population.

[56] The three starting assumptions are: (1) common Pb is negligible as compared to the amount of thorogenic and uranogenic lead [Parrish, 1990]; (2) no radiogenic Pb loss has occurred since system closure, Pb content is not significantly affected by diffusion [e.g., Cocherie et al., 1998; Crowley and Ghent, 1999; Zhu and O'Nions, 1999]; (3) a single age is involved at the size level of each individual spot analysis. After comparison with conventional isotopic U-Pb age determinations, it is now accepted that EPMA resolution allows to avoid inclusions and altered domains that could potentially contain common Pb. Systematic BSE study was performed to investigate monazite micro-texture for all analyzed grains.

A2. Ion Microprobe Dating

[57] Zircons were dated using the ion microprobe (IMS 1270) at CNRS, CRPG Nancy (France), according to the procedure described by Deloule et al. [2002]. The areas analyzed (~25 μm) were selected after studying images of the grains obtained by cathodoluminescence and by transmitted light microphotography. The determination of the $^{238}U/^{206}Pb$ ratio necessitated the external calibration of the measurements with the aid of a particularly homogeneous standard zircon of known composition: the geostandard 91500 zircon from Ontario (Canada) dated at 1065 Ma [Wiedenbeck et al., 1995]. In general, areas very rich in U (>2000–3000 ppm) were not selected in order to avoid, first, moving away from the area of validity of the U-Pb calibration line and, secondly, the risk of losses of radiogenic Pb, in relation to the metamictization. For the relatively recent zircons (<1000 Ma), the imprecision of the $^{206}Pb/^{204}Pb$ ratio becomes critical; one then uses the Concordia diagram [Tera and Wasserburg, 1972], modified by Compston et al. [1989], in which one plots the $^{207}Pb/^{206}Pb$ and $^{238}U/^{206}Pb$ ratios, not corrected for common Pb. In the absence of common Pb, the analyses of areas not affected by thermal events subsequent to the crystallization of the zircon or by inherited cores are spread along this Concordia [Willliams, 1998]. Although the variable quantities of common Pb adversely affect the values of the two ratios, these kind of points form a straight line passing through the composition of common Pb ($^{207}Pb/^{206}Pb$) at the estimated age of the system given, in a first approximation, by the average $^{238}U/^{206}Pb$ ages stemming from the concordant analyses. The extrapolation of this line on the Concordia defined the sought age. This is what is called a correction of common Pb by the ^{207}Pb method and not by the ^{204}Pb method, as in the case of the conventional diagram. Using this correction method, one calculates the $^{206}Pb^*/^{238}U$ (Pb* = radiogenic Pb) ratios for each point. Whatever the used analytical approach, all the calculations were made at 2σ (95% confidence limit) using the ISOPLOT program (version 2) of Ludwig [2000]. On the other hand, in the case of the data obtained using the ion microprobe, the uncertainties are given at 1σ in the corresponding table and, in the same way, the error ellipses are given at 1σ in order to make the figures easier to read.

Acknowledgments

[58] C. Gilles (BRGM) and O. Rouer (ISTO) are acknowledged for their technical assistance in operating EPMA. The authors also acknowledge M. Champenois, E. Deloule, and D. Mangin (CRPG-CNRS-Nancy) in operating the IMS 1270. E. Bé Mézème thanks the Conseil Régional du Centre for providing a scholarship during his Ph.D. Field expenses and laboratory analyses have been funded by the Programme de la Carte Géologique de France, managed in BRGM. Constructive comments on an earlier draft by anonymous reviewers are acknowledged.

References

Ballèvre, M., J. Marchand, G. Godard, J.-C. Goujou, and R. Wyns (1994), Eo-Hercynian events in the Massif Armoricain, in Pre-Mesozoic Geology of France and Related Areas, edited by J. D. Keppie, pp. 183−194, Springer, New York.

Bellot, J.-P. (2001), La structure de la croûte varisque du Sud-Limousin (Massif Central français) et ses relations avec les minéralisations aurifères tardi-orogéniques: apport des données géologiques, gîtologiques, géophysiques et de la modélisation 3D, Ph.D. thesis, 320 pp., Univ. Montpellier, Montpellier, France.

Berthier, F., J. L. Duthou, and M. Roques (1979), Datation géochronologique Rb/Sr sur roches totales du granite de Guéret (Massif Central). Age fini-Dévonien de mise en place de l'un de ses faciès types, Bull. Bur. Rech. Geol. Min. Fr., 1, 31–42.

Bosse, V., G. Féraud, G. Ruffet, M. Ballèvre, J.-J. Peucat, and K. de Jong (2000), Late Devonian subduction and early-orogenic exhumation of eclogite facies rocks from the Champtoceaux Complex (Variscan Belt), Geol. J., 35, 297–325.

Boutelier, D. (2004), La modélisation expérimentale tridimensionnelle thermo-mécanique de la subduction continentale et l'exhumation des roches de ultra haute pression/basse température, PhD. thesis, 202 pp., Univ. Nice, Nice, France.

Boutelier, D., and A. Chemenda (2003), 3D thermo-mechanical experimental modelling of exhumation of UHP/LT rocks, paper presented at AGU-EGS-EUG Joint Assembly, AGU, Nice.

Boutelier, D., A. Chemenda, and J. P. Burg (2003), Subduction versus accretion of intra-oceanic volcanic arc: Insights from thermo-mechanical analogue experiments, Earth Planet. Sci. Lett., 212, 31–45.

Boutin, R., and R. Montigny (1993), Datation $^{39}Ar/^{40}Ar$ des amphibolites du complexe leptyno-amphibolique du plateau d'Aigurande: collision varisque à 390 Ma dans le Nord-Ouest du Massif Central français, C. R. Acad. Sci., Ser. 2, 316, 1391–1398.

Carswell, D. A., and R. Y. Zhang (1999), Petrographic characteristics and metamorphic evolution of ultrahigh-pressure eclogites in plate collision belts, Int. Geol., Rev., 41, 781–798.

Cartannaz, C., P. Rolin, A. Cocherie, D. Marquer, O. Legendre, C. M. Fanning, and P. Rossi (2006), Characterization of wrench tectonics from dating syn- to post-magmatism in the

north-western French Massif Central, Int. J. Earth Sci., 96, 271–287, doi:10.1007/s00531-0066-0101-y.

Cartier, C. (2002), Structure de l'Unité de St-Georges-sur-Loire et du Domaine Ligérien (Massif Armoricain), Ph. D. thesis, 309 pp., Univ. d'Orléans, Orléans, France.

Cartier, C., and M. Faure (2004), Structure and Geodynamic evolution of the Gondwana-Armorica boundary in the Ligerian domain (Armorican massif, France), Int. J. Earth Sci., 93, 945–958, doi:10.1007/S00531-0040398-3.

Cartier, C., M. Faure, and H. Lardeux (2001), The Hercynian orogeny in the South Armorican Massif (France): Rifting and welding of continental stripes, Terra Nova, 13, 143–149.

Chemenda, A., M. Mattauer, J. Malavieille, and A. Bokun (1995), A mechanism for syn-collisional exhumation and associated normal faulting: Results from physical modeling, Earth Planet. Sci. Lett., 132, 225–232.

Chemenda, A. I., M. Mattauer, and A. N. Bokun (1996), Continental Subduction and a Mechanism for Exhumation of High-Pressure Metamorphic Rocks: New Modelling and Field Data from Oman, Earth Planet. Sci. Lett., 143, 173–182.

Chemenda, A., P. Matte, and V. Sokolov (1997), A model of Paleozoic obduction and exhumation of high-pressure/low temperature rocks in southern Urals, Tectonophysics, 276, 217–227.

Chemenda, A., D. Hurpin, J.-C. Tang, and J.-F. Stephan (2001), Impact of arc-continent collision on the conditions of burial and exhumation of UHP/LT rocks: Experimental and numerical modeling, Tectonophysics, 342, 137–161.

Chopin, C. (2003), Ultrahigh-pressure metamorphism: Tracing continental crust into the mantle, Earth Planet. Sci. Lett., 212, 1–14.

Cocherie, A., and F. Albarède (2001), An improved U-Th-Pb age calculation for electron microprobe dating of monazite, Geochim. Cosmochim. Acta, 65, 4509–4522.

Cocherie, A., and O. Legendre (2007), Potential minerals for determining U-Th-Pb chemical age using electron microprobe, Lithos, 93, 288–309.

Cocherie, A., O. Legendre, J.-J. Peucat, and A. Kouamelan (1998), Geochronology of polygenetic monazites constrained by in situ electron microprobe Th-U-total Pb determination: Implications for lead behaviour in monazite, Geochim. Cosmochim. Acta, 62, 2475–2497.

Cocherie, A., E. Be Mezeme, O. Legendre, M. Fanning, M. Faure, and P. Rossi (2005), Electron microprobe dating as a tool for understanding closure of U-Th-Pb system in monazite from migmatite, Am. Mineral., 90, 607–618.

Cogné, J. (1966), Une nappe cadomienne de style pennique: la série cristallophylienne de Champtoceaux en bordure méridionale du synclinal d'Ancenis (Bretagne-Anjou), Bull. Serv. Carte Geol. Alsace Lorraine, 19, 107–136.

Cogné, J. (1974), Le Massif Armoricain, in Géologie de la France edited by J. Debelmas, pp. 105−161, Doin, Paris.

Compston, W., I. S. Williams, J. L. Kirschvink, Z. Zhang, and G. Ma (1989), Zircon U-Pb ages for Early Cambrian time scale, J. Geol. Soc., 149, 171–184.

Costa, S., and H. Maluski (1988), Datations par la méthode $^{39}Ar/^{40}Ar$ de materiel magmatique et métamorphique paléozoïque provenant du forage de Couy-Sancerre (Cher, France) Programme GPF, C. R. Acad. Sci., Ser. II, 306, 351–356.

Crowley, J. L., and E. D. Ghent (1999), An electron microprobe study of the U-Th-Pb systematics of metamorphosed monazite: the role of Pb diffusion versus overgrowth and recrystallization, Chem. Geol., 157, 285–302.

Deloule, E., P. Alexendrov, A. Cheilletz, B. Laumonier, and P. Barbey (2002), In situ U-Pb zircon ages for early Ordovician magmatism in the Eastern Pyrénées, France: The Canigou orthogneiss, Geol. Rundsch., 91, 398–405.

Dewey, J. (1988), Extensional collapse of orogens, Tectonics, 7, 1123–1139.

Diot, H. (1980), Recherches structurales et stratigraphiques dans la partie orientale du domaine ligérien (Massif armoricain), Ph. D. thesis, 160 pp., Univ. de Nantes, Nantes, France.

Dubreuil, M. (1986), Evolution géodynamique du Paleozoïque ligérien (Massif Armoricain), Ph.D. thesis, 258 pp., Univ. de Nantes, Nantes, France.

Ducrot, J., J. R. Lancelot, and J. Marchand (1983), Datation U-Pb sur zircon de l'éclogite de la Borie (Haut Allier, France) et consequences sur l'évolution ante-hercynienne de l'Europe occidentale, Earth Planet Sci. Lett., 62, 385–394.

Duthou, J. L., M. Chenevoy, and M. Gay (1994), Age Rb/Sr Dévonien moyen des migmatites à cordiérite du Lyonnais (Massif Central français), C. R. Acad. Sci., Ser. II, 319, 791–796.

Faure, M. (1995), Late orogenic carboniferous extensions in the Variscan French Masssif Central, Tectonics, 14, 132–153.

Faure, M., C. Leloix, and J.-Y. Roig (1997), L'évolution polycyclique de la chaıcirc;ne hercynienne, Bull. Soc. Geol. Fr., 168, 695–705.

Faure, M., E. Be Mézème, M. Duguet, C. Cartier, and J.-Y. Talbot (2005), Paleozoic tectonic evolution of medio-Europa from the example of the French Massif Central and Massif Armoricain, in The Southern Variscan Belt, edited by R. Carosi et al., J. Virtual Explorer, 19, Paper 4.

Floc'h, J.-P. (1983), La série métamorphique du Limousin central, Ph. D. thesis, 445 pp., Univ. Limoges, Limoges, France.

Godard, G. (2001), The Les Essarts eclogite-bearing metamorphic complex (Vendée, southern Massif Armoricain, France, Geol. Fr., 19–51, 2001.

Godard, G., and H. Van Roermund (1995), Deformation induced clinopyroxene fabrics from eclogites, J. Struct. Geol., 17, 1425–1443.

Granet, M., S. Judenherc, and A. Sourriau (2000), Des images du système lithosphere-asthénosphère sous la France et leurs implications géodynamiques: l'apport de la tomography télésismique et de l'anisotropie sismique, Bull. Soc. Geol. Fr., 171, 149–167.

Lafon, J.-M. (1986), Géochronologie U-Pb appliquée à deux segments du Massif Central français. Le Rouergue oriental et le Limousin central, Ph. D. thesis, 1152 pp., Univ. Montpellier, Montpellier, France.

Lagarde, J.-L. (1978), La déformation des roches dans les domains à schistosité subhorizontale. Application à la nappe du Canigou-Roc de France (Pyrénées Orientales) et au Complexe de Champtoceaux (Massif Armoricain), Ph. D. thesis, 170 pp., Univ. Rennes, Rennes, France.

Lardeux, H., and P. Cavet (1994), Paleozoic of the Ligerian Domain, in Pre-Mesozoic Geology of France and Related Areas, edited by J. D. Keppie, pp. 152−156, Springer, New York.

Lardeaux, J.-M., P. Ledru, I. Daniel, and S. Duchene (2001), The Variscan French Massif Central—A new addition to the ultra-high pressure metamorphic “club”: Exhumation processes and geodynamic consequences, Tectonophysics, 332, 143–167.

Lasnier, B., A. Leyreloup, and J. Marchand (1973), Découverte d'un granite “charnockitique” au sein de gneiss oeillés, Perspectives nouvelles sur l'origine de certaines leptynites du Massif Armoricain Méridional (France), Contrib. Mineral. Petrol., 41, 131–144.

Ledru, P., J. M. Lardeaux, D. Santallier, A. Autran, J.-M. Quenardel, J.-P. Floc'h, G. Lerouge, N. Maillet, J. Marchand, and A. Ploquin (1989), Où sont les nappes dans le Massif Central français?, Bull. Soc. Geol. Fr., 8, 605–618.

Le Gall, B., S. Loboziak, and S. Le Herissé (1992), Le flanc sud du synclinorium carbonifère de Châteaulin (Massif armoricain, France): une bordure de bassin réactivée en contexte décro-chevauchant, Bull. Soc. Geol. Fr., 163, 13–26.

Leloix, C., M. Faure, and J. L. Feybesse (1999), Hercynian polyphase tectonics in north-east French Massif Central: The closure of the Brévenne Devonian-Dinantian rift, Int. J. Earth Sci., 88, 409–421.

Lister, G. S., and G. A. Davis (1989), The origin of metamorphic core complexes and detachment faults formed during Tertiary continental extension in the northern Colorado River region, USA, J. Struct. Geol., 11, 65–94.

Liu, J. G., T. Tsujimori, R. Y. Zhang, I. Katayama, and S. Maruyama (2004), Global UHP metamorphism and continental subduction/collision: The Himalayan model, Int. Geol. Rev., 46, 1–27.

Ludwig, K. R. (2000), Users Manual for Isoplot/Ex. version 2.00, A geochronological toolkit for Microsoft Excel, Spec. Publ. 1a, 43 pp., Berkeley Geochronol. Cent., Berkeley, Calif.

Malavieille, J. (1993), Late orogenic extension in mountain belts: Insights from the Basin and Range and the Late Paleozoic Variscan Belt, Tectonics, 12, 1115–1130.

Marchand, J. (1981), Ecaillage d'un “mélange tectonique” profond: le complexe cristallophyllien de Champtoceaux (Bretagne Méridionale), C. R. Acad. Sci., Ser. II, 293, 223–228.

Matte, P. (1986), La chaîne varisque parmi les chaînes paléozoïques péri-atlantiques, modèle d' évolution et position des grands blocs continentaux au Permo-Carbonifère, Bull. Soc. Geol. Fr., 8, 9–24.

Matte, P. (2001), The Variscan collage and orogeny (480–290 Ma) and the tectonic definition of the Armorica microplate: A review, Terra Nova, 13, 122–128.

McKerow, W. S., C. McNiocaill, P. E. Ahlberg, G. Clayton, C. J. Cleal, and M. C. Eagar (2001), The Late Palaeozoic relations between Gondwana and Laurussia, in Orogenic Processes, Quantification and Modelling in the Variscan Belt, edited by W. Franke et al., Geol. Soc. Spec. Publ., 179, 9–20.

Paquette, J.-L. (1987), Comportement des systèmes isotopiques U-Pb et Sm-Nd dans le métamorphisme éclogitique, Mem. Doc. CAES 14, 190 pp., Com. Local d'Action Soc., Rennes, France.

Paquette, J.-L., J.-J. Peucat, J. Bernard-Griffith, and J. Marchand (1985), Evidence for old Precambrian relics shown by U-Pb zircon dating of eclogites and associated rocks in the Hercynian Belt of South Brittany, France, Chem. Geol., 52, 203–216.

Paquette, J.-L., P. Monchoux, and M. Couturier (1995), Geochemical and isotopic study of a norite-eclogite transition in the European Variscan Belt: Implications for U-Pb systematics in metabasic rocks, Geochim. Cosmochim Acta, 59, 1611–1622.

Paris, F., and M. Robardet (1990), Early Palaeozoic paleobiogeography of the Variscan Belt, Tectonophysics, 177, 193–213.

Parrish, R. R. (1990), U-Pb dating of monazite and its implication to geological problems, Can. J. Earth Sci., 27, 1431–1450.

Pearce, J. A., N. B. W. Harris, and A. G. Tindle (1984), Trace element discrimination for the tectonic interpretation of granitic rocks, J. Petrol., 25, 956–983.

Pelhate, A. (1994), Carboniferous of the Armorican Massif, in Pre-Mesozoic Geology in France and Related Areas, edited by J. D. Keppie, pp. 162–168, Springer, New York.

Peucat, J.-J., P. Vidal, G. Godard, and B. Postaire (1982), Precambrian U-Pb zircon ages in eclogites and garnet pyroxenites from south Brittany (France): An old oceanic crust in the west European Hercynian Belt?, Earth Planet Sci. Lett., 60, 70–78.

Pin, C., and J. Lancelot (1982), U-Pb dating of an early Paleozoic bimodal magmatism in the French Massif Central and its further metamorphic evolution, Contrib. Mineral. Petrol., 79, 1–12.

Pin, C., and J.-J. Peucat (1986), Ages des épisodes de métamorphisme paléoïques dans le Massif central et le Massif armoricain, Bull. Soc. Geol. Fr., 8, 461–469.

Pommier, A., A. Cocherie, and O. Legendre (2002), EPMA dating Users' manual: Age calculation from electron probe microanalyzer measurements of U-Th-Pb, internal report, Bur. de Rech. Geol. et Min., Orléans, France.

Robardet, M. (2003), The Armorica "microplate": Fact or fiction? Critical review of the concept and contradictory palaeobiogeographical data, Palaeogeogr. Palaeoclimatol. Palaeoecol., 195, 125–148.

Roig, J.-Y., and M. Faure (2000), La tectonique cisaillante polyphasée du Sud-Limousin, Bull. Soc. Geol. Fr., 171, 295–307.

Roig, J. Y., M. Faure, and C. Truffert (1998), Folding and granite emplacement inferred from structural, strain, TEM, and gravimetric analyses: The case study of the Tulle antiform, SW French Massif Central, J. Struct. Geol., 20, 1169–1189.

Rolet, J. (1982), La Phase Bretonne en Bretagne: état des connaissances, Bull. Soc. Geol. Mineral. Bretagne, 14, 63–71.

Santosh, M., A. S. Collins, I. Tamashiro, S. Koshimoto, Y. Tsutsumi, and K. Yokoyama (2006), The timing of ultrahigh-temperature metamorphism in Southern India: U-Th-Pb electron microprobe ages from zircon and monazite in sapphirine-bearing granulites, Gondwana Res., 10, 128–155.

Suzuki, K., and M. Adachi (1991), Precambrian provenance and Silurian metamorphism of the Tsubonosawa paragneiss in the South Kitakami terrane, northeast Japan, revealed by the chemical Th-U-total Pb isochron ages of monazite, zircon and xenotime, Geochem. J., 25, 11–37.

Tera, F., and G. F. Wasserburg (1972), U-Th-Pb systematics in three Apollo 14 basalts and the problem of initial Pb in lunar rocks, Earth Planet Sci Lett., 14, 281–304.

Vidal, P., J.-J. Peucat, and B. Lasnier (1980), Dating of granulites involved in the Hercynian fold-belt of Europe: An example taken from the granulite-facies orthogneiss at La Picherais, Southern Armorican Massif, France, Contrib. Mineral. Petrol., 72, 283–289.

Wendt, I., and C. Carl (1991), The statistical distribution of the mean squared weighted deviation, Chem. Geol., 86, 275–285.

Wernicke, B., and B. C. Burchfiel (1982), Modes of extensional tectonics, J. Struct. Geol., 4, 105–115.

Wiedenbeck, M., P. Allé, F. Corfu, W. L. Griffin, M. Meier, F. Oberli, A. von Quadt, J. C. Roddick, and W. Spiegel (1995), Three natural zircon standards for U-Th-Pb, Lu-Hf, trace element and REE analysis, Geostand. Newsl., 19, 1–23.

Willliams, I. S. (1998), U-Th-Pb Geochronology by Ion Microprobe, Rev. Ecol. Geol., 7, 1–35.

Zhu, X. K., and R. K. O'Nions (1999), Zonation of monazite in metamorphic rocks and its implications for high temperature thermochronology: A case study from the Lewisian terrain, Earth Planet. Sci. Lett., 171, 209–220.

Figures

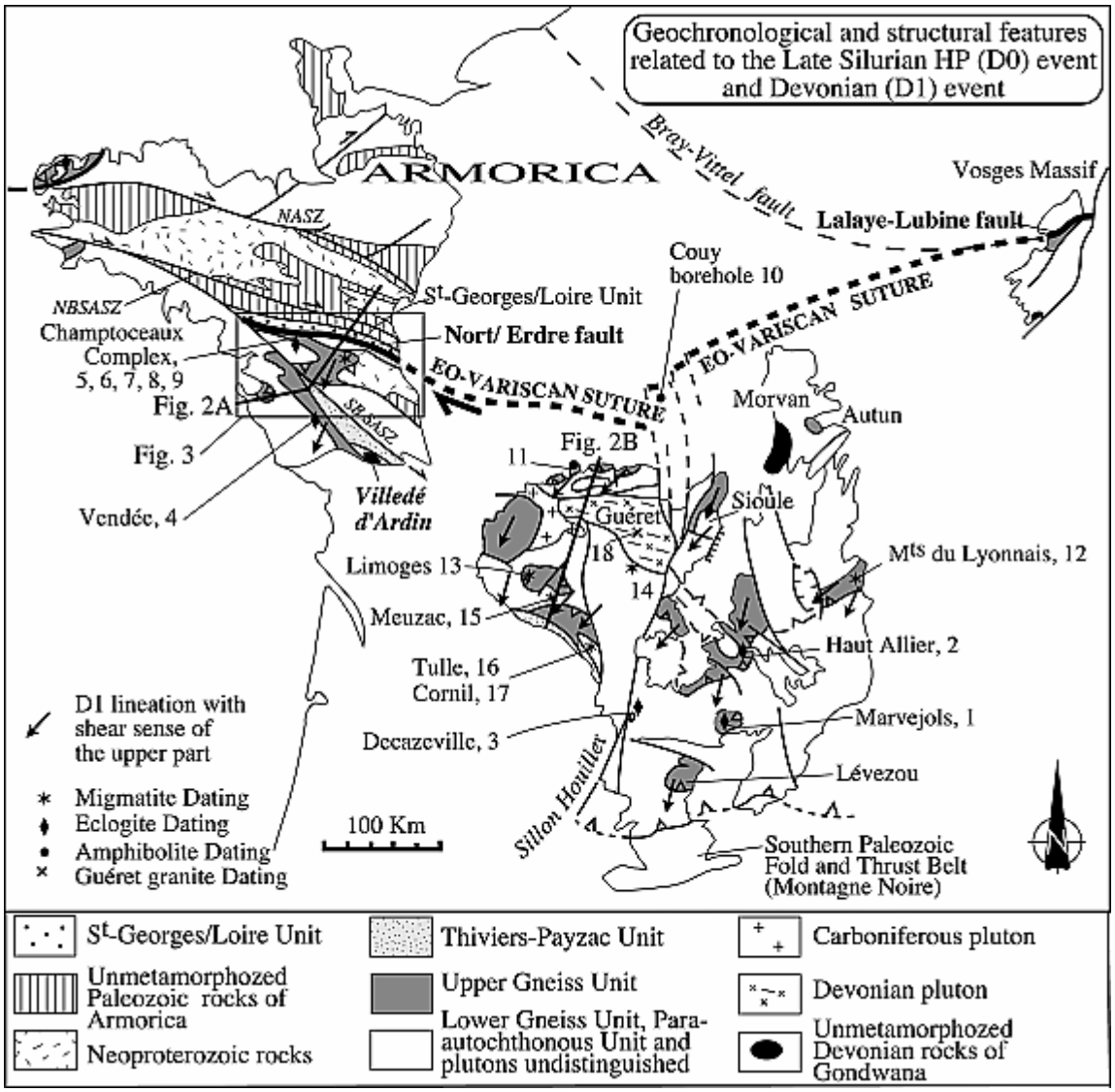

Figure 1. Simplified structural map of the Massif Armoricain and Massif Central with emphasis on the pre-Carboniferous events. The numbers refer to available dates for the HP metamorphism, anatexis in the UGU and LGU, and amphibolitization of eclogites presented in Table 1. The pattern of stretching and mineral lineation developed during the D1 event (see text) is also provided. NASZ, North Armorican Shear Zone; NBSASZ, North Branch of the South Armorican Shear Zone; SBSASZ, South Branch of the South Armorican Shear Zone. Carboniferous plutons and structures are omitted

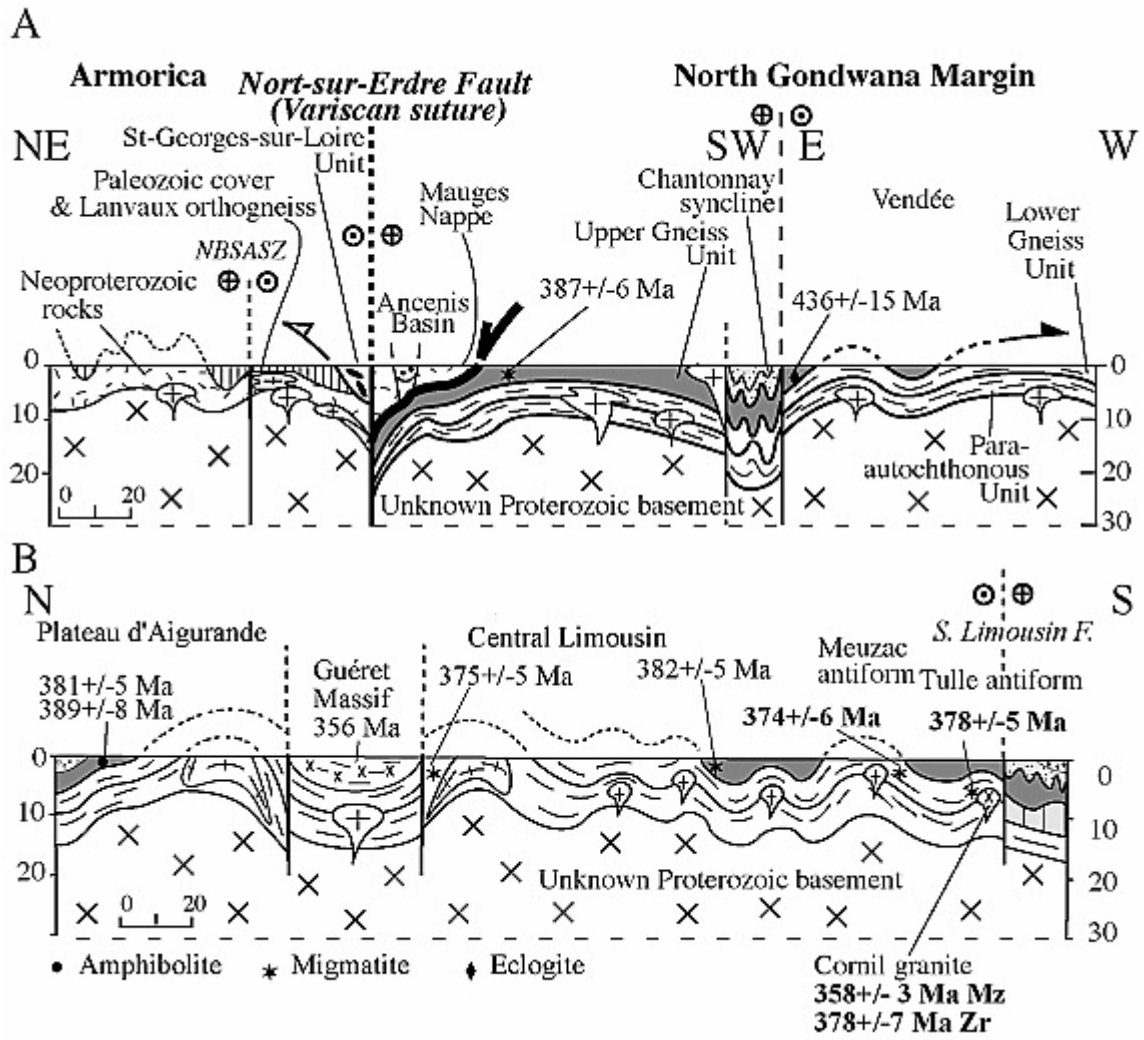

Figure 2. Crustal-scale cross sections, located in Figure 1, showing the stack of Variscan nappes in the Massif Armoricain and Massif Central. (a) The Nort-sur-Erdre suture separates Armorica and North Gondwana Margin continental domains, to the north and south, respectively. Armorica is the overriding plate formed by upright folded Paleozoic series. The St-Georges-sur-Loire Unit is a block-in-matrix series with exotic blocks supplied by a southern Missing Domain. South of the suture zone, the North Gondwana Margin is a stack of nappes, namely, from bottom to top, the Para-autochthonous Unit, the Lower Gneiss Unit (LGU), and the Upper Gneiss Unit (UGU). An Ophiolitic Nappe corresponding to the remnant of the Medio-European Ocean (thick line) is overthrust by the Mauges Nappe. (b) In the Limousin area, only N. Gondwana Margin nappes (UGU, LGU, and Para-autochthonous Unit) are recognized. In both areas, upright folds deform the initially flat-lying thrust faults, and the edifice is cut by wrench faults developed in Carboniferous. Numbers in the two sections indicate the radiometric ages: bold numbers are the new ages presented in this paper and normal numbers are ages available in the literature (see Table 1 for details).

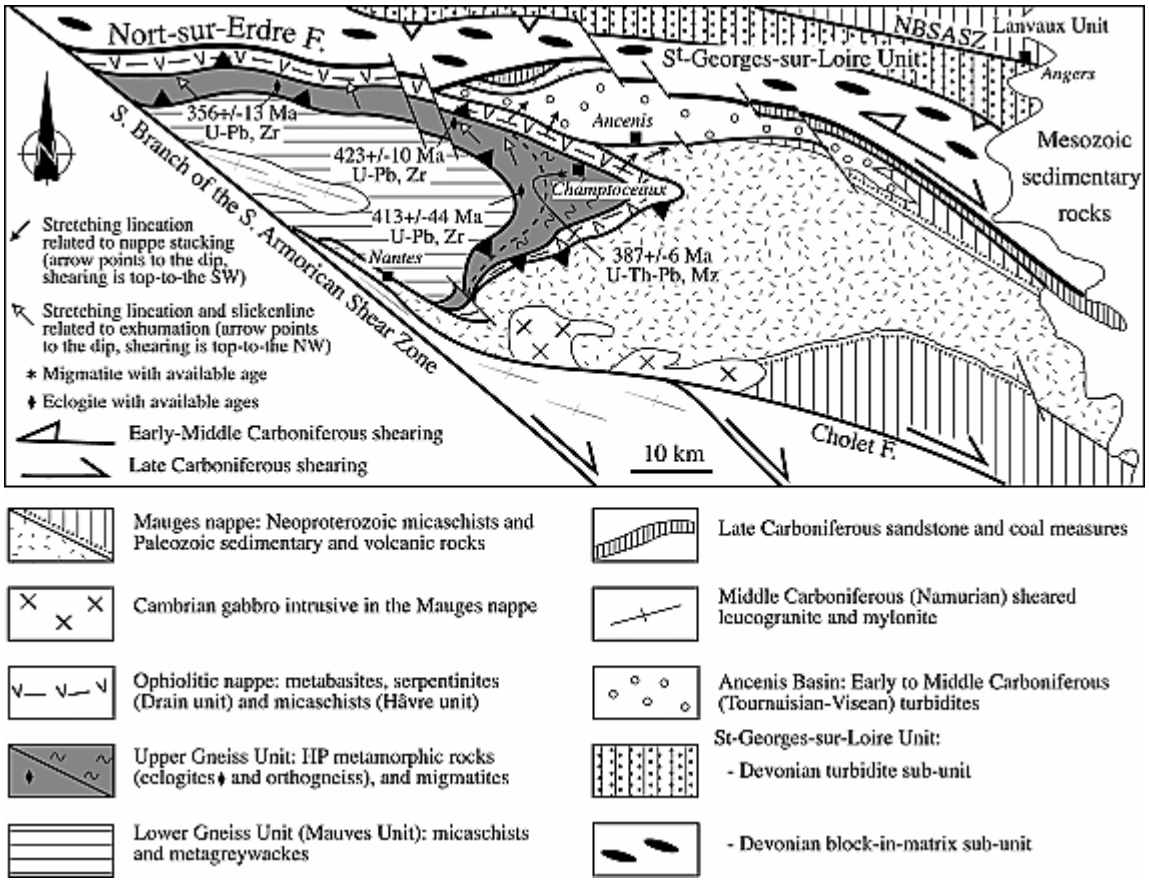

Figure 3. Structural map of the Armorica-Gondwana suture zone in the south part of the Massif Armoricain showing the stack of nappes. The Nort-sur-Erdre fault represents the surface expression of the suture zone. Numbers are radiometric ages presented in Table 1 (Zr, zircon; Mz, monazite).

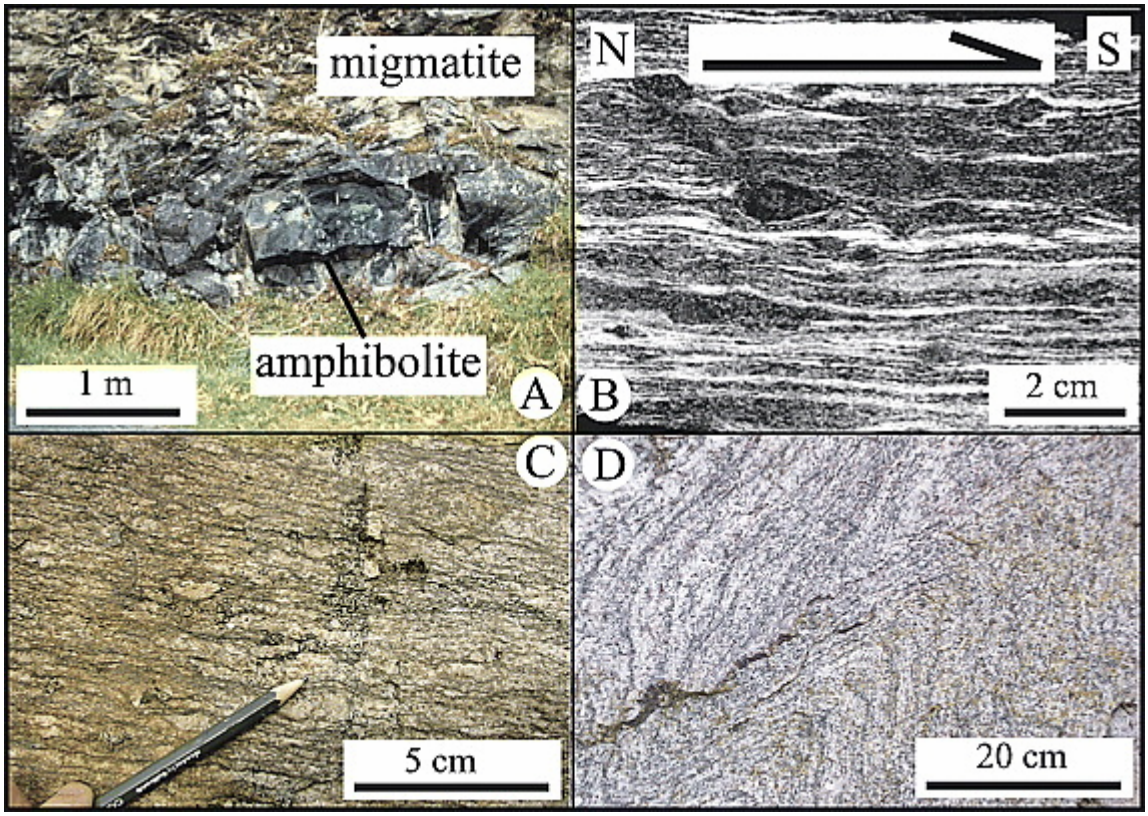

Figure 4. Examples of representative field features of migmatites and ophiolites. (a) Migmatite of the UGU enclosing a meter-sized block of amphibolite formed by retrogression of eclogite and interpreted as unmelted protolith (Plateau d'Aigurande, N. Limousin). (b) Mylonitized ophiolitic gabbro with top-to-the-south sigmoidal clasts of pyroxene (Ophiolitic Nappe, Champtoceaux Complex). (c) Foliated migmatite with centimeter-sized K-feldspar augen (sample Li 5) forming the host rock of the Cornil granite (Tulle antiform). (d) Folded metatexite (sample Li 9) in the southern limb of the Meuzac antiform.

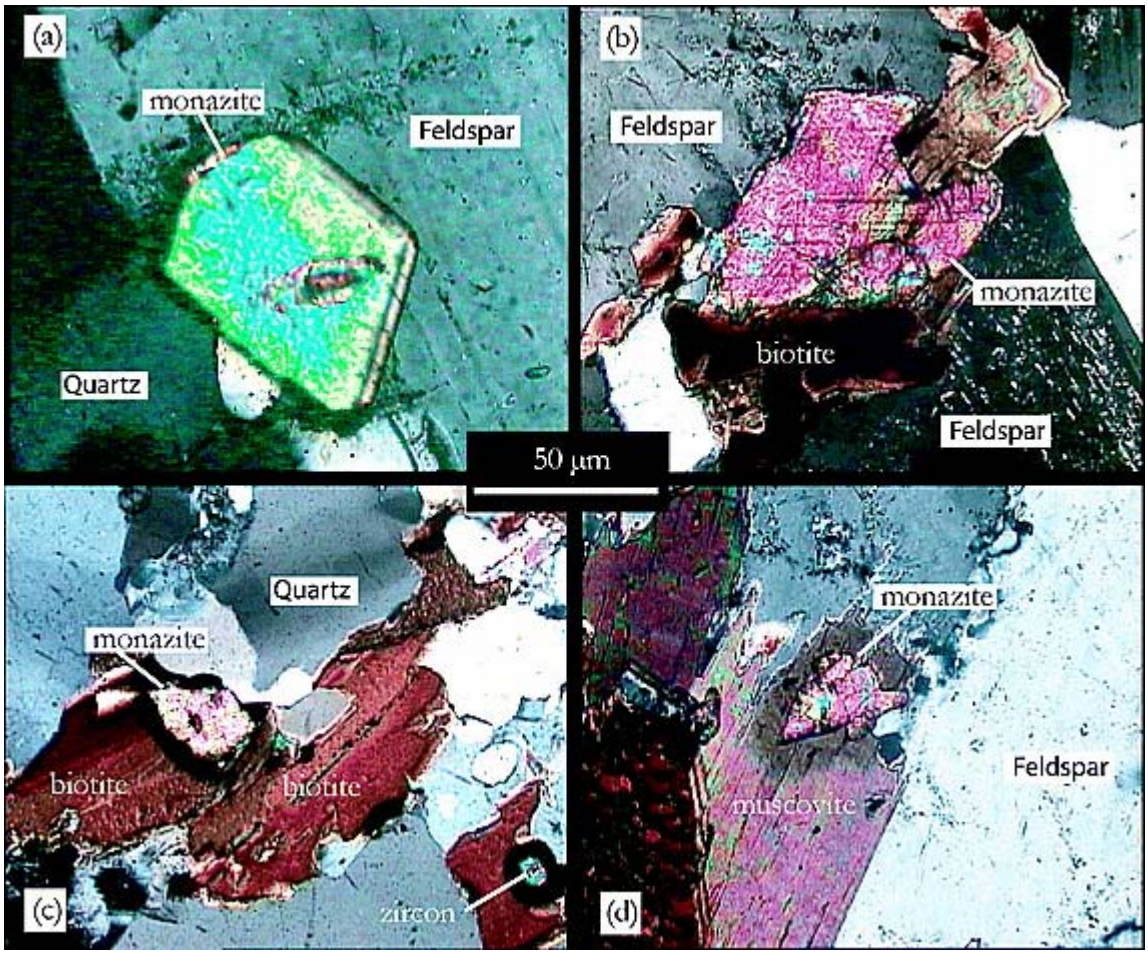

Figure 5. Micrographs showing the textural relationships between monazite and other mineral phases in the dated samples. (a) Euhedral grain in migmatite (sample Li 5), (b) subhedral grain in Cornil granite (sample Li 6), (c) monazite inclusion in biotite in migmatite (sample Li 9), and (d) monazite inclusion in biotite in migmatite (sample Li 5); note the pleochroic halo around monazite.

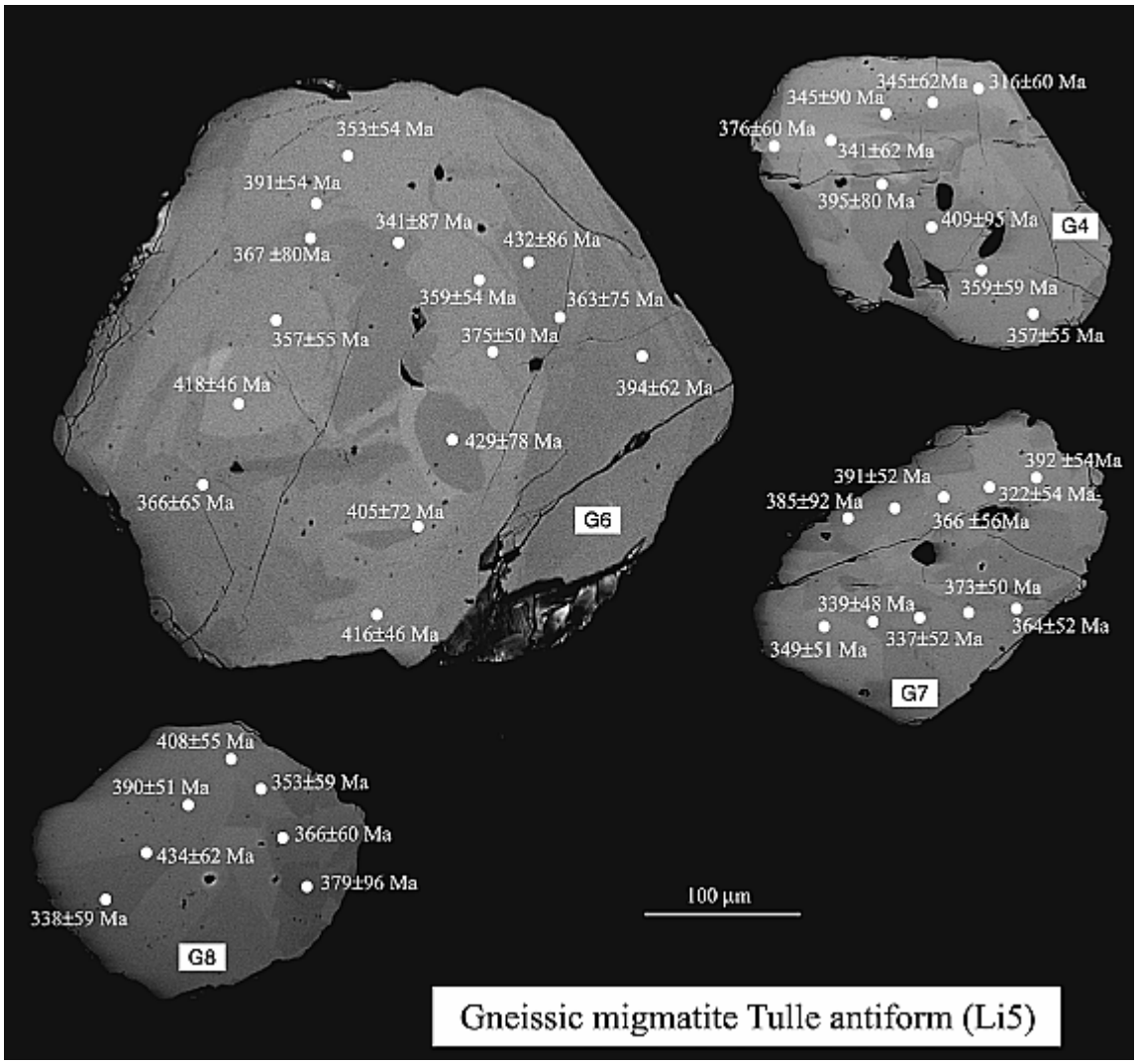

Figure 6. SEM BSE image of dated monazite grains extracted from sample Li 5 (located in Figure 1). Grains are subhedral, fractured, and display a complex patchy zoning unrelated to grain growth (see text for discussion). For clarity, only half of the age spots are shown in the grain images. Complete data set is provided in auxiliary material. The corresponding isochron plot is given in Figure 8.

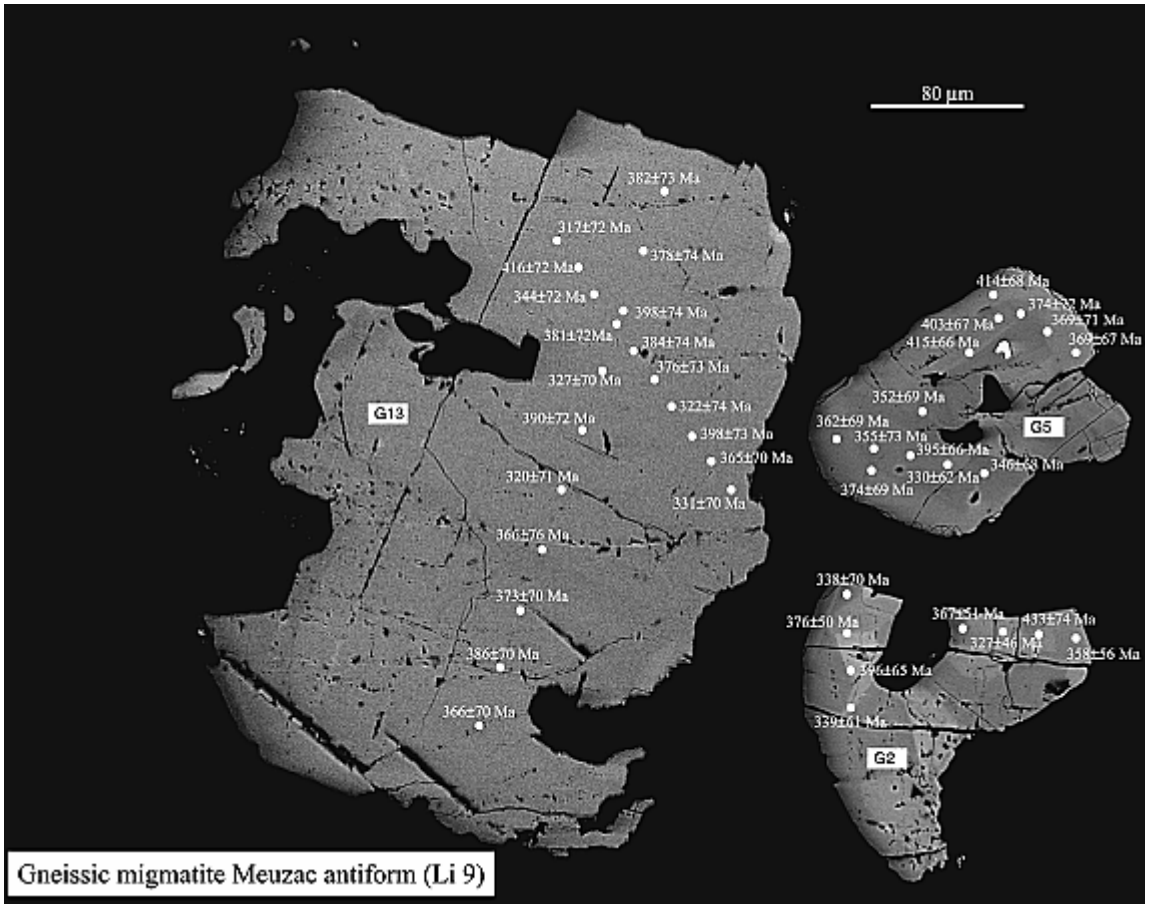

Figure 7. SEM BSE image of dated monazite grains extracted from sample Li 9 (located in Figure 1). Grains are skeletal with limited patchy zoning. For clarity, only half of the age spots are shown in the grain images. Complete data set is provided in auxiliary material. The corresponding isochron plot is given in Figure 9.

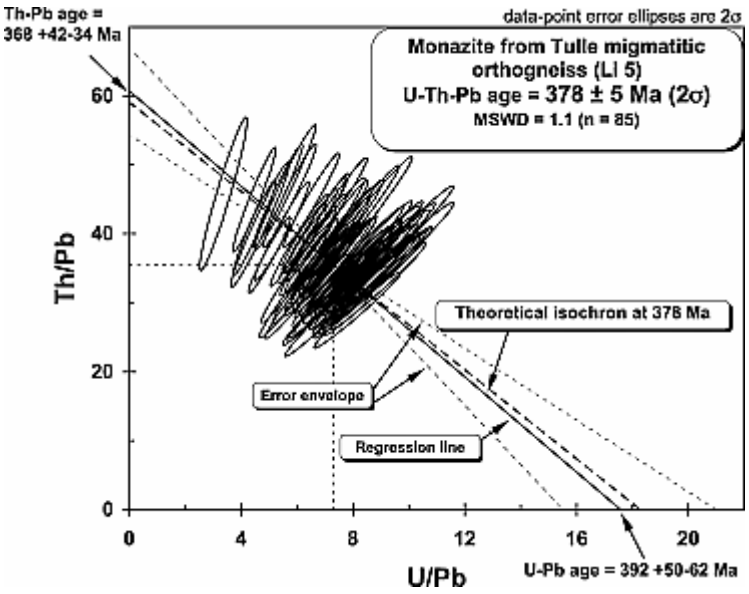

Figure 8. Plot of Th/Pb versus U/Pb for 4 monazite grains from the Tulle migmatitic orthogneiss (Li 5). The intercept ages are similar within the analytical error, validating the calculation of the mean age at the centroid of the population: 378 ± 5 Ma. Note that the regression line is subparallel to the theoretical isochron at 378 Ma. In simple terms, the isochron is located between the two error hyperbolas that define the error envelope.

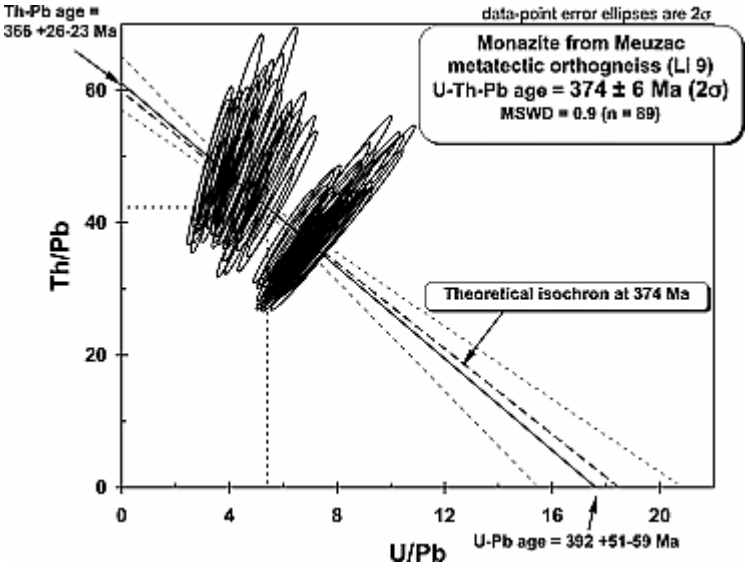

Figure 9. Plot of Th/Pb versus U/Pb for four monazite grains from the Meuzac metatectic orthogneiss (Li 9). The intercept ages are similar within the analytical error, validating the calculation of the mean age at the centroid of the population: 374 ± 6 Ma.

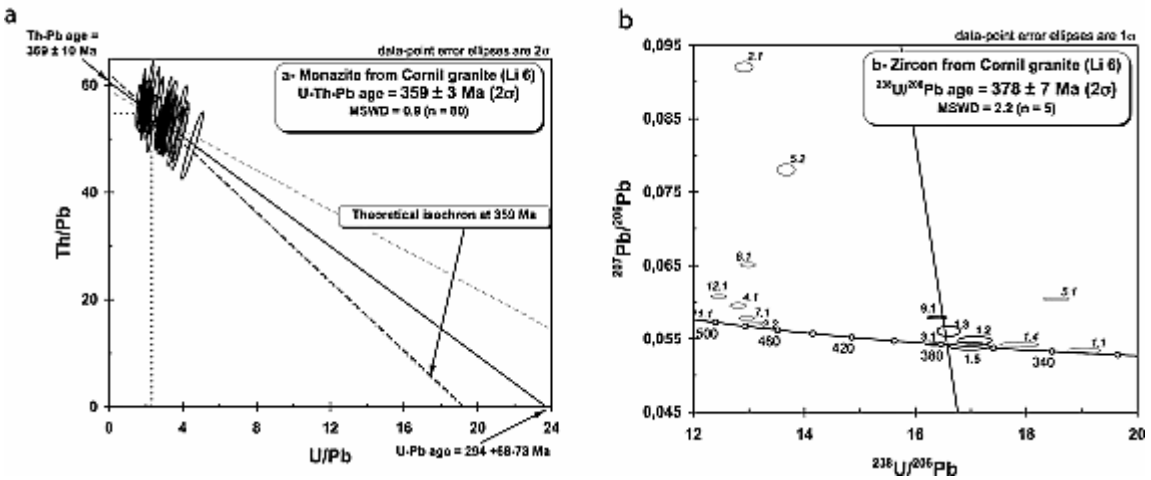

Figure 10. Geochronological data from the Cornil granite (sample Li 6). (a) U-Th-Pb age from monazite indicating a crystallization age of 359 ± 3 Ma; (b) Tera-Wasserburg plot for ion microprobe dating of zircon grains. The number near each ellipse corresponds to analytical point of Table 3. Bold numbers are those considered for average intercept age calculation; italic ones were not considered. The 378 ± 7 Ma age is interpreted as the age of the protolith of the Cornil granite. The ~480 Ma age is considered as the age of the Ordovician granite, which is the protolith of the migmatite. The analyses giving ages younger than 360 Ma are supposed to have undergone radiogenic Pb loss.

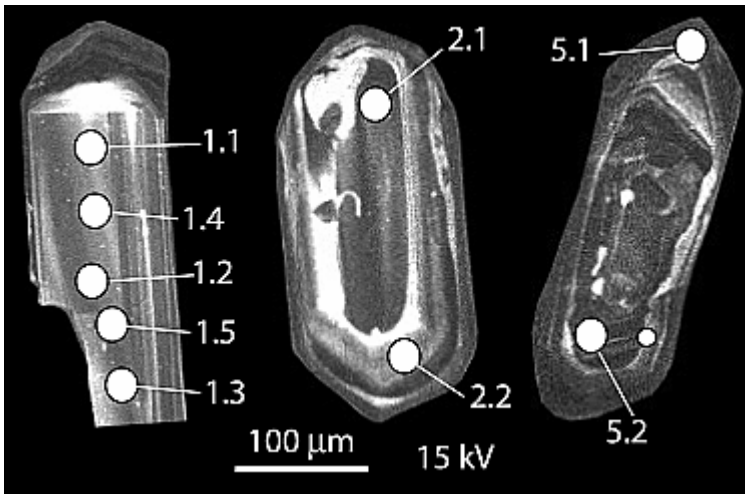

Figure 11. Cathodoluminescence images of representative zircons from the Cornil granite (sample Li 6). Grain 1 is part of a larger well-crystallized grain without inherited core; grain 2 shows a typical magmatic growth zoning; grain 5 exhibits an inherited core and recrystallized rim. The analytic data corresponding to each measurement are given in Table 3

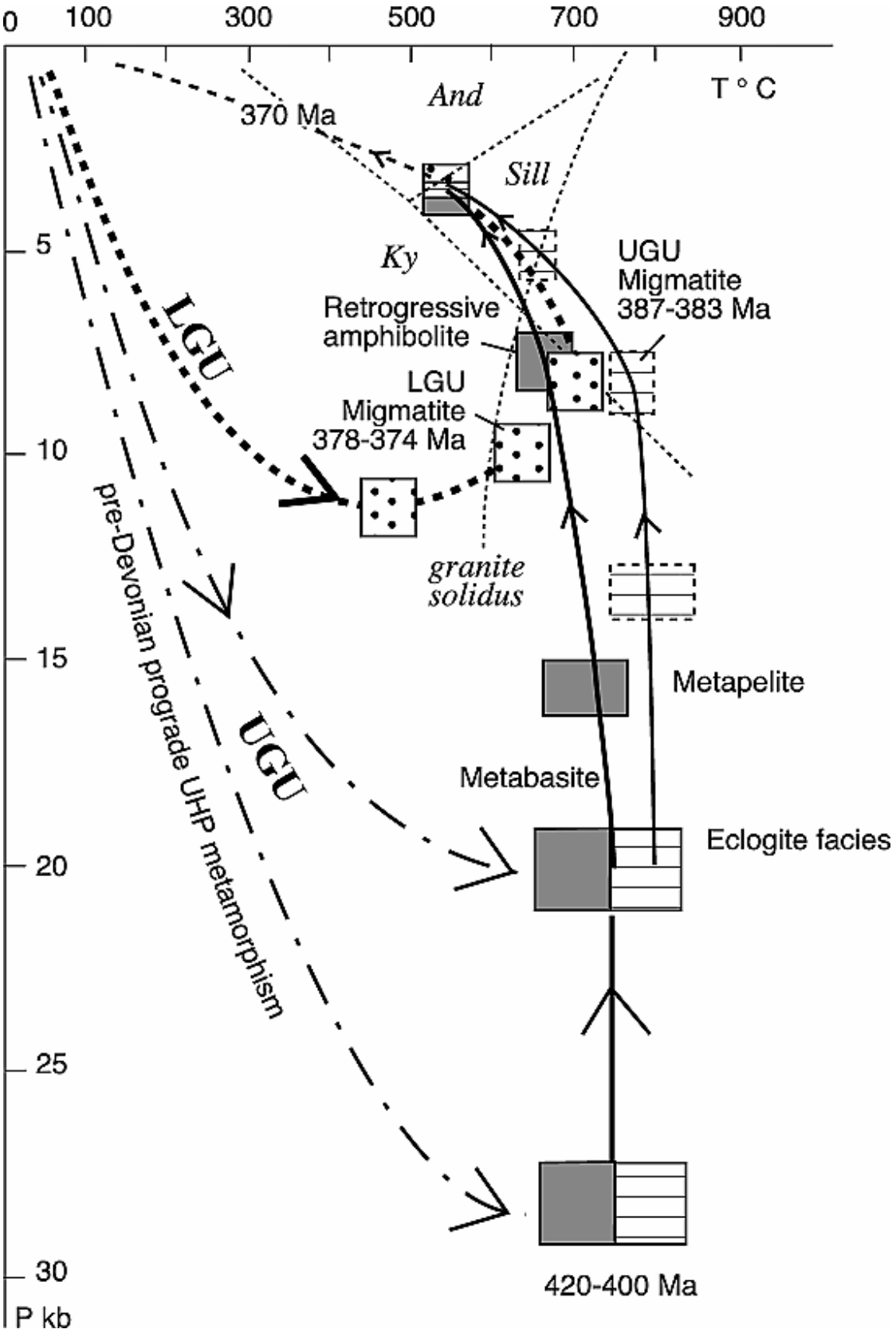

Figure 12. Synthetic P-T-t paths for UGU and LGU. P and T estimates are compiled from Floc'h [1983], Ballèvre et al. [1994], Roig and Faure [2000], Godard [2001], Bellot [2001], and Lardeaux et al. [2001]. Note that the prograde paths are not documented. Dotted pattern, LGU; grey pattern, mafic rocks in UGU; striped pattern, felsic and pelitic rocks in UGU.

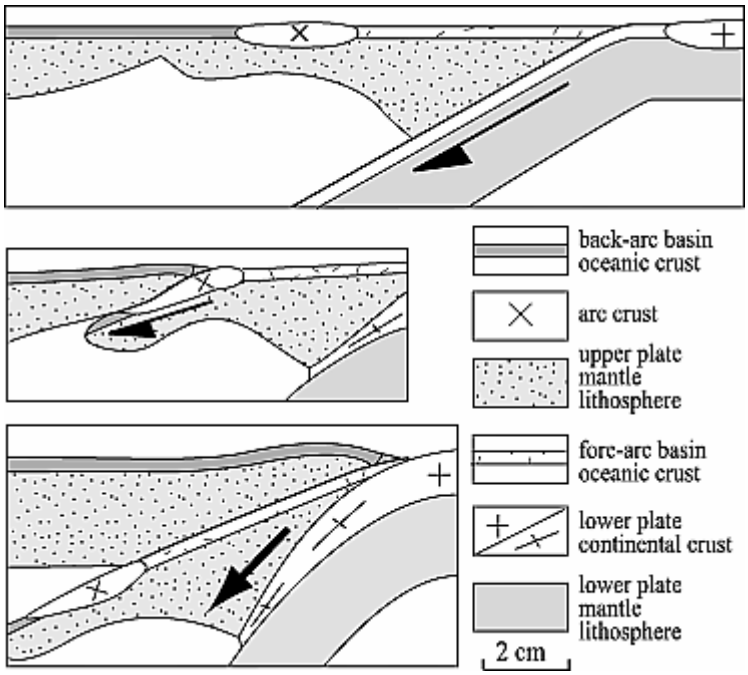

Figure 13. Drawing from the pictures of experiment 2 of Boutelier et al. [2003] showing the major features of continental subduction below an upper plate composed of an arc and back-arc system. Under a high-compression mode, the hot crust of a young back-arc basin fails and the thin and strong arc crust is completely subducted below the upper plate.

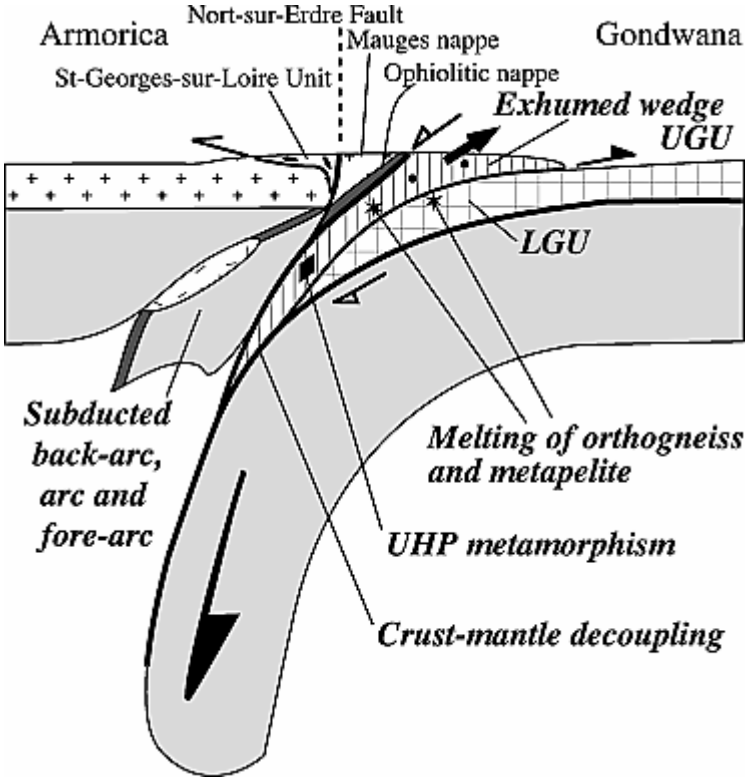

Figure 14. Lithosphere-scale interpretative cross section of the geometry of the Armorica-Gondwana convergent zone in Middle Devonian. The back-arc basin (Layon rift) and the Ligerian arc have been subducted below Armorica. The St-Georges-sur-Loire Unit with

block-in-matrix formation is the only remain of the back-arc basin. The basement Mauges Nappe overthrusts the Ophiolitic Nappe. The UHP rocks of the UGU occur in a crustal wedge partly migmatized during their exhumation. In the footwall of the UGU wedge, the LGU rocks are also partly migmatized during their exhumation. The Carboniferous events, namely, pluton emplacement, strike-slip faulting, ductile shearing in the Para-autochthonous Unit, and opening of the Ancenis basin, are not represented.

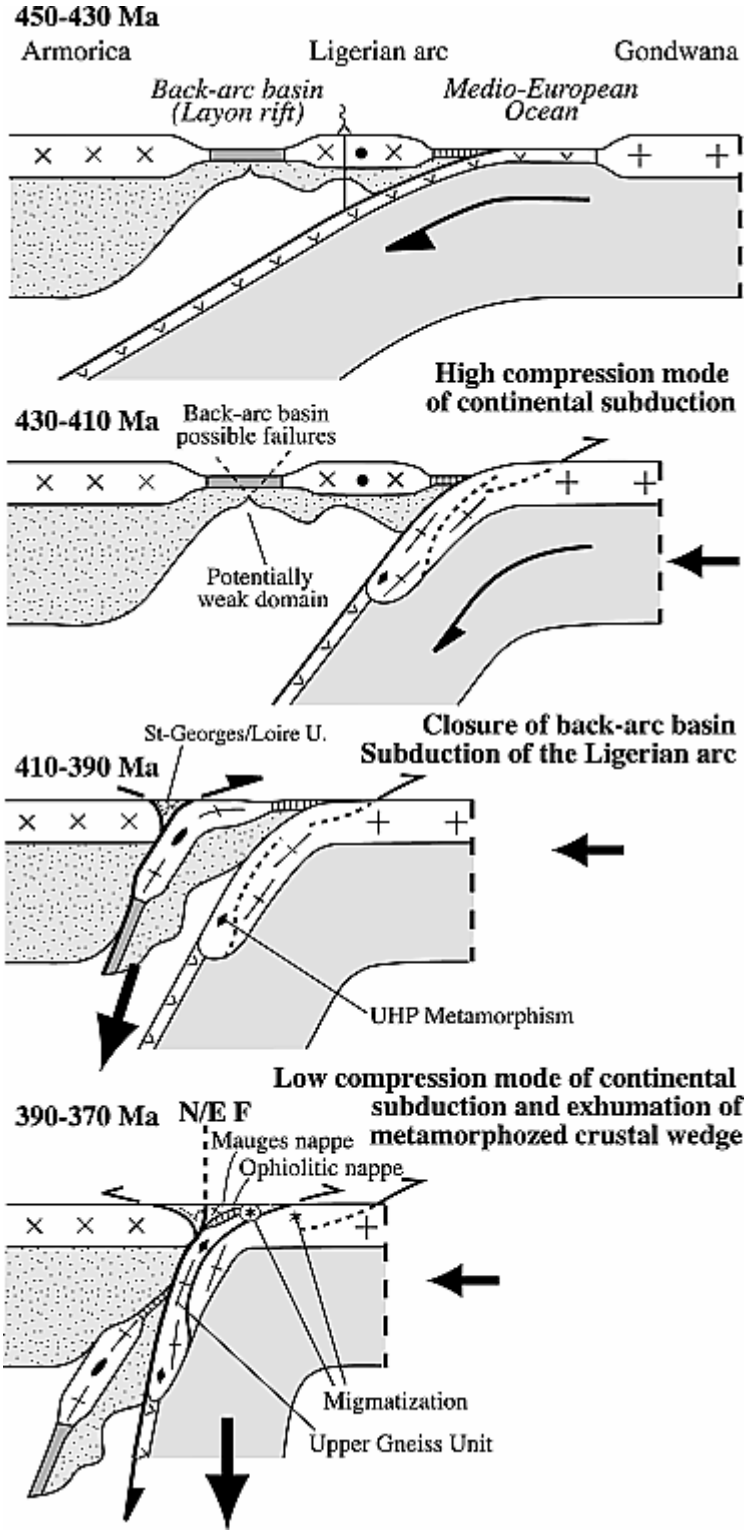

Figure 15. Geodynamic evolution model of the early stages of the French Variscan Belt. Around 450–430 Ma, Gondwana is converging toward Armorica through the subduction of the Medio-European Ocean. The Armorica margin is composed of a magmatic arc and a back-arc called the Ligerian arc and Layon Rift, respectively. Around 430–410 Ma, continental subduction of the North Gondwana margin is responsible for the development of HP to UHP metamorphism in the Gondwana continental crust. The high-compression mode induces a compressive state of stress in the overriding plate. The Armorica plate fails in the back-arc basin area. Around 410–390 Ma, the arc-back arc domain is subducted below Armorica. The St-Georges-sur-Loire Unit represents a relict of the back-arc basin. At some point during the arc plate subduction, the continental subduction switches to the low-compression regime allowing the exhumation of the UGU crustal wedge. Pressure decrease coeval with the exhumation of the UHP rocks leads to anatexis of the Gondwana continental crust between 390 Ma and 370 Ma.

Tables

Table 1. Geochronological Data Available for UGU and LGU in the French Massif Central (MC) and Massif Armoricain (MA)[a]

Massif	Locality	Point in Figure 1	Rock Type	Dated Mineral	Method	Age (in Ma)	Reference
UGU Tectonic Unit							
MC	Marvejols	1	Eclogite	zircon	U-Pb	415 ± 6	Pin and Lancelot [1982]
	Haut-Allier	2	Eclogite	zircon	U-Pb	432+20/−10	Ducrot et al. [1983]
	Decazeville	3	Eclogite	zircon	Pb-Pb	413 ± 23	Paquette et al. [1995]
				whole rock + garnet	Sm-Nd U-Pb	408 ± 7 436 ± 15	
MA	Vendée	4	Eclogite	zircon			Peucat et al. [1982]
	Champtoceaux complex	5	Eclogite	zircon	U-Pb	413 ± 44	Paquette et al. [1985]
		6	Eclogite	Zircon	U-Pb	356 ± 8	Bosse et al. [2000]
		7	Eclogite	WR + garnet + cpx	Sm-Nd	362 ± 25	
		8	Orthogneiss	zircon	U-Pb	423 ± 10	Vidal et al. [1980]
		9	Migmatite	monazite	U-Th-Pb	387 ± 6	Cocherie et al. [2005]
MC	Couy borehole	10	Amphibolite	biotite	$^{40}Ar/^{39}Ar$	385 ± 8	Costa and Maluski [1988]
			Amphibolite	hornblende	$^{40}Ar/^{39}Ar$	383 ± 8	
	Plateau d'Aiguran de	11	Amphibolite	biotite	$^{40}Ar/^{39}Ar$	381 ± 5	Boutin and Montigny [1993]
			Amphibolite	hornblende	$^{40}Ar/^{39}Ar$	389 ± 8	
	Lyonnais	12	Migmatite	whole rock	Rb-Sr	384 ± 16	Duthou et al. [1994]
	Limoges area	13	Migmatite	zircon	U-Pb	382 ± 5	Lafon [1986]
LGU Tectonic Unit							
MC	S. Guéret	14	Migmatite	monazite	U-Th-Pb	375 ± 5	A. Cocherie (unpublished data)
	Limousin (Meuzac area)	15	Migmatite	monazite	U-Th-Pb	374 ± 6	this study
	Limousin (Tulle area)	16	Migmatite	monazite	U-Th-Pb	378 ± 5	this study
	Limousin (Cornil pluton)	17	Granite	monazite	U-Th-Pb	359 ± 3	this study
				zircon	U-Pb SHRIMP	378 ± 4	
	Limousin Guéret pluton	18	Granite	whole rock	Rb-Sr	356 ± 10	Berthier et al. [1979]
				monazite	U-Th-Pb	352 ± 5	Cartannaz et al. [2006]
				zircon	U-Pb SHRIMP	351 ± 5	Cartannaz et al. [2006]

[a]Age uncertainties are given at 2σ level.

Right-click (PC) or CTRL-click (Mac) to download tab-delimited version: table2.txt

Table 2. Average Chemical Composition of Analyzed Monazites[a]

	Pb ± σ Standard Deviation (ppm)	U ± σ Standard Deviation (ppm)	Th ± σ Standard Deviation (ppm)	Th/U ± σ Standard Deviation	Isochron Age ± 2σ (Ma)	n
Tulle migmatitic orthogneiss (Li 5)	1096 ± 216	8070 ± 2016	39504 ± 8225	5.2 ± 1.7	378 ± 5	85
Meuzac metatectic orthogneiss (Li 9)	942 ± 163	5268 ± 1189	40192 ± 9486	8.3 ± 3.2	374 ± 6	89
Cornil granite (Li 6)	2632 ± 588	6347 ± 836	143772 ± 34725	23.1 ± 6.4	359 ± 3	80
[a]Note that n denotes the number of individual analyses taken into account for isochron age calculation.						

Right-click (PC) or CTRL-click (Mac) to download tab-delimited version: table3.txt

Table 3. U/Pb Analyses of Zircons of the Cornil Granite Obtained From IMS 1270 Ion Probe

							Total				Radiogenic		Age (Ma)	
Grain. Spot	U (ppm)	Th (ppm)	Th/U	Pb* (ppm)	$^{204}Pb/^{206}Pb$	f_{206} [a] %	$^{238}U/^{206}Pb$	±Uncertainty[b]	$^{207}Pb/^{206}Pb$	±Uncertainty[b]	$^{206}Pb/^{238}U$[c]	±Uncertainty[b]	$^{206}Pb/^{238}U$	±Uncertainty[b]
1.1	458	123	0.27	21	0.00005	0.04	19.05	0.24	0.05335	0.00037	0.0525	0.0006	330	4
1.2	574	189	0.33	29	-	0.11	17.08	0.25	0.05477	0.00045	0.0585	0.0008	366	5
1.3	201	49	0.25	10	-	0.23	16.60	0.17	0.05603	0.00056	0.0601	0.0006	376	4
1.4	542	172	0.32	26	-	0.08	17.88	0.28	0.05418	0.00027	0.0559	0.0009	351	5
1.5	465	147	0.32	24	-	0.001	16.97	0.30	0.05399	0.00041	0.0589	0.0010	369	6
2.1	531	374	0.71	35	0.00245	4.36	12.91	0.13	0.09204	0.00055	0.0741	0.0007	461	4
2.2	474	81	0.17	31	0.00000	0.06	13.10	0.11	0.05707	0.00019	0.0763	0.0007	474	4
3.1	3797	209	0.06	199	0.00004	0.00	16.36	0.14	0.05425	0.00015	0.0611	0.0005	382	3
4.1	1091	91	0.088	73	0.00016	0.33	12.80	0.11	0.05953	0.00028	0.0779	0.0007	483	4
5.1	1897	495	0.26	88	0.00056	0.89	18.54	0.19	0.06042	0.00015	0.0535	0.0005	336	3
5.2	1206	396	0.33	76	0.00144	2.71	13.67	0.13	0.07804	0.00063	0.0711	0.0007	443	4
6.1	640	41	0.06	42	0.00044	1.04	12.98	0.11	0.06507	0.00024	0.0762	0.0007	474	4
7.1	719	80	0.11	48	0.00018	0.14	12.97	0.11	0.05780	0.00021	0.0770	0.0007	478	4
9.1	342	661	0.1	179	0.0003	0.45	16.39	0.15	0.0578	0.00014	0.0607	0.0005	380	3

	4		9		2				8					
10.1	2498	975	0.39	127	0.00596	10.90	16.88	0.25	0.14146	0.00127	0.0528	0.0008	332	5
11.1	3176	1576	0.50	223	0.00001	0.01	12.23	0.10	0.05743	0.00009	0.0817	0.0007	506	4
12.1	529	127	0.24	36	0.00022	0.44	12.46	0.12	0.06076	0.00018	0.0799	0.0007	496	4

[a]Here f_{206}% denotes the percentage of ^{206}Pb that is common Pb.
[b]Uncertainties given at one σ level.
[c]Correction for common Pb made using the measured $^{238}U/^{206}Pb$ et $^{207}Pb/^{206}Pb$ ratios following Tera and Wasserburg [1972] as outlined by Willliams [1998].